2010

A PCA based method for image and video pose sequencing

James Massaro

A PCA Based Method for Image and Video Pose Sequencing

by

James Massaro

A Thesis Submitted

in

Partial Fulfillment

of the

Requirements for the Degree of MASTER OF SCIENCE

in

Electrical Engineering

Approved By:

PROF. _____

Thesis Advisor- Dr. Raghuveer Rao

PROF. _____

Thesis Committee Member- Dr. Sohail Dianat

PROF. _____

Thesis Committee Member- Dr. Ferat Sahin

PROF. _____

Electrical Engineering Department Head- Dr. Sohail Dianat

DEPARTMENT OF ELECTRICAL AND MICROELECTRICAL ENGINEERING

COLLEGE OF ENGINEERING

ROCHESTER INSTITUTE OF TECHNOLOGY

ROCHESTER, NEW YORK

February 2010

THESIS RELEASE PERMISSION

ROCHESTER INSTITUTE OF TECHNOLOGY

DEPARTMENT OF ELECTRICAL AND MICROELECTRICAL ENGINEERING

Title of Thesis:

A PCA Based Method for Image and Video Pose Sequencing

I, James Massaro, hereby grant permission to Wallace Memorial Library of R.I.T. to reproduce my thesis in whole or in part. Any reproduction will not be for commercial use or profit.

Signature _____

Date

2010

Dedication

I would like to dedicate this thesis to my fiancé Stephanie and my parents because of all their support and patients.

Acknowledgments

First, I would like to thank my advisor, Dr. Raguhveer Rao for his instruction and assistance. I would also like to thank my committee members Dr. Ferat Sahin and the Department Head, Dr. Sohail Dianat for finding time to listen and make recommendations for a better thesis. A special thanks to Dr. Ferat Sahin for encouraging me to do my best with writing to make this thesis something I will be proud of for the rest of my career and life.

Abstract

Problems exist in image sequence processing that require an ordered set of object views. In some cases, multiple angled images are acquired in random order and the angle of view information is not available. When this occurs, the poses have to be put into proper order. For example, in databases containing images of an object or scene taken over a period of time, each image pose or angled-view with respect to the camera or scene is unknown. This is important to achieve a complete or partial three-dimensional reconstruction. Other applications exist in photogrammetry, machine vision, computer-aided design, and military intelligence. The main contribution of this thesis is an automated method for ordering images of random object views. This method uses Principal Component Analysis (PCA) and a confidence metric in eigenspace. The confidence measure is based on local curvature and correlation of the estimated pose trajectory in a multidimensional manifold. The use of the confidence metric is for detecting areas in the manifold where poses appear similar and ordering becomes difficult. It has been extended for use with synchronized double and multiple camera system by providing a basis for camera selection, choosing the most salient camera view for pose ordering. By adding multiple cameras, a high pose estimation accuracy can be achieved. This thesis compares other classification and recognition methods such as the Scale Invariant Feature Transform (SIFT) and Laplacian Eigenmaps. The SIFT algorithm struggles with pose sequencing because it computes local feature spaces for each image and does not consider the entire set of images. Laplacian eigenmaps show better results for ordering, but close analysis show it is better suited for clustering poses than sequencing. Results for ordering many set of objects, theoretical development, and comparison of methods is presented in this research.

Chapter 1

Introduction

1.1 Overview

Digital image processing (DIP) is a field that utilizes mathematical theories and models with various applications. DIP is a broad term that includes several more specific areas of research. A few areas of research in DIP include but are not limited to pattern recognition, computer vision,artificial intelligence, surveillance, automation, and 3D modeling. These areas of research utilize motion estimation, and image segmentation to perform a recognition task. For example, law enforcement uses facial recognition software to identify criminals [1].

The ultimate goal for most advanced DIP systems is to control machines to perform a specific task or to notify the user of a specific event. Recognition tasks notify the user when a specific object has been identified. One problem inherent to performing these tasks is recognition at varying pose or view-angle. An object that is not perfectly aligned with the training data will exhibit different spatial features and cause errors because of

shape and illumination differences. One proposed solution for solving this problem is to construct a training database that encompasses the entire 360° rotation of the object. However, a continuous sampling of an objects rotation cannot be achieved. This is called pose resolution, and it leads to another possible source of error. To fix this problem, a method for pose recognition must be developed.

The most common way to perform pose recognition is by constructing a database of angled-views. This can be done in two ways, either by manually taking images or videos of an object in a laboratory, or through an unsupervised method of actively acquiring data through a strategically placed camera(s). The unsupervised method has two drawbacks:

1. It is difficult and time consuming to place labels on the information that is being acquired, and

2. the pose database is unordered and needs to be reordered to verify that there is enough data for proper pose recognition. The amount of data needed for object pose recognition is determined by its pose resolution.

Other supervised methods capable of recognizing an object in a scene at different scales and poses have been developed by [2, 3]. These types of algorithms can recognize the object up to certain pose angle until features become occluded or unrecognizable from illumination changes.

This thesis proposes an unsupervised object pose ordering algorithm seen briefly in the research by Massaro *et al.* [4]. It uses a confidence metric to find possible pose errors because of indistinguishing views. This method is extended to a multiple camera framework for improved sequencing. The proposed method could also be used in other applications such as pose recognition, image matching, aerial surveillance, and photogrammetry.

These topics will be discussed in more detail within the following chapter.

1.2 Random Object Poses

This section discusses the definition of an ordered set of object poses and an unordered set of random object poses. Proceeding this is the motivation for pose ordering. This includes database sequencing and 3D model construction, unsupervised learning for facial databases, and path planning for unmanned aerial vehicles (UAVs). These are all possible applications for ordered sets of object poses seen as an improvement to current algorithms.

1.2.1 What are random object poses?

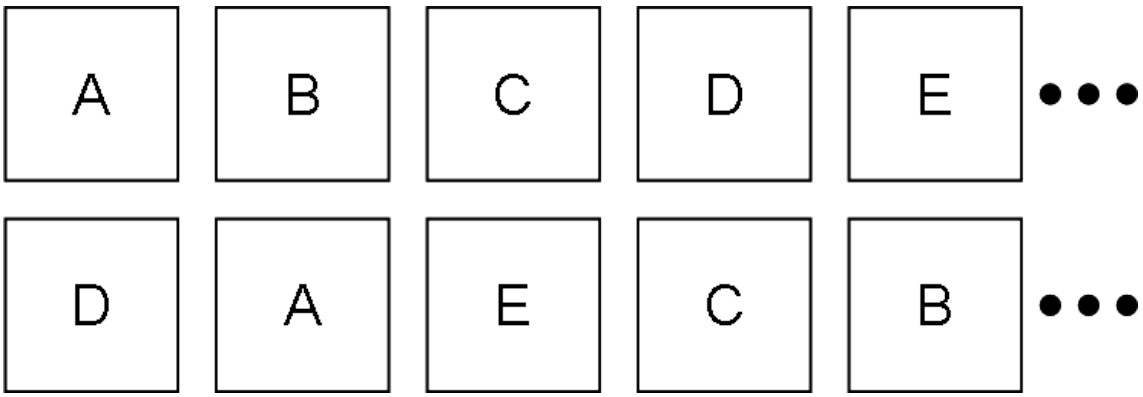

Figure 1.1: Example of a video sequence (top) and a randomized video sequence (bottom).

The pose of an object is the view-angle at which an object is observed. Each angled-view or pose induces illumination changes and 2D shape variation creating different observable features. The continuous transition of these observable features is a set of ordered object

poses. Monotonically changing angled-views of an object can be captured by a by a stationary video camera and a turntable. The motion video captures an ordered set of object poses. Contrarily, an unordered set of object poses are non-monotonically changing angled-views of an object. The non-monotonicity of the view-angle is a random set of object poses. This can be seen in Figure 1.1 where the top figure is an ordered set of poses, and the bottom sequence is a random set of poses.

1.2.2 Image Databases

The initial motivation for pose ordering was to create a way to automatically find stereo matching images in a series of random, unordered images. Stereo matching pairs can be used to create a rough 3D model of the scene or object. The disorderedness of image poses in the same scene occurs when images are taken at different times under varying perspective. These types of images are required for capturing perspectives of a scene for constructing a 3D model.

Random views of objects or scenes can be found in many real-world applications. Some of these situations are found in remote sensing, and aerial surveillance. The situation of randomness occurs frequently in these situations because of the variability in viewing angle of air-born vehicles. The need for an alternative image-perspective based algorithm arises because GPS and geo-referencing is not enough or may not have been available to reorder images. The research by O'Dwyer *et al.* [5] use old imagery from 1953-1972 when the technology was not available for image geo-referencing. Furthermore, these types of images are taken over a period of time under varying circumstances for the type of mission. For this reason, the perspectives of the same area result in different images that may need to be ordered for photogrammetry or change detection.

Further research has indicated the necessity of ordered images for photogrammetric methods [6]. It has been stated in this research that automated ordering of random image databases would reduce the effort of ordering manually, which is costly and time consuming. Moreover, this research states that these processes struggle with making measurements from images with unordered data sets.

1.2.3 Machine Learning

Another motivation for object pose ordering is for supervised pose recognition of objects. These methods refer to the design of a training databases from random views of an object. The research in [7] outlines a system for the unsupervised acquisition of human faces for a humanoid robot. The method explains that this can be achieved when objects and faces are presented randomly to a camera. Each object or face is grouped into a pose database. The database requires a method for unsupervised ordering to develop accurate training data. Human interaction is optional for acquiring labels to faces. The human interaction is involved in this method is known as inductive learning, while the faces are acquired and ordered in an unsupervised fashion. Chapter 2 discusses how knowledge of the relative order of the object or face poses is important for training.

1.3 Thesis Organization

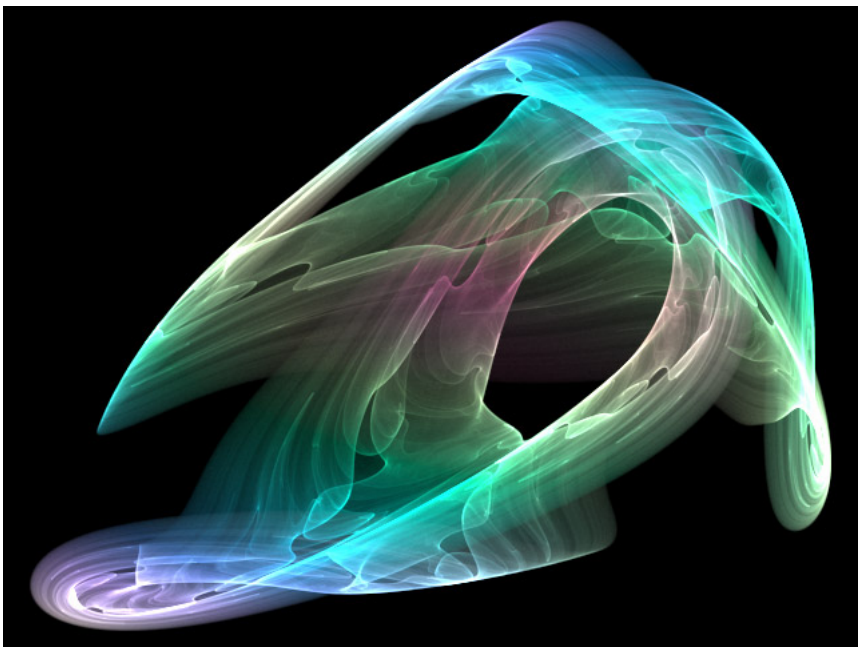

Figure 1.2: A visual example of a manifold. This image was obtained under the GNU Free Document License

The following chapters will explain the research path for object pose ordering. Chapter 2 discusses the previous work conducted that relates to this thesis. This includes 3D model construction methods, image matching, object recognition, image manifolds, and object pose recognition methods. An example of a manifold can be seen in Figure 1.2. The research in this section leads to the development of the methodology that will be used for object pose ordering. Chapter 2 introduces the problem of pose ordering in terms of Principal Component Analysis (PCA) space. Furthermore, this chapter describes the methods used for traversing a manifold, and why PCA is chosen. Chapter 3 gives a

detailed explanation of the method, including mathematical derivations and explanations of hardware configuration and metrics used for object pose ordering. Chapter 4 contains results obtained for single and two camera pose ordering, as well as results for a pose clustering method. Chapter 5 contains the summary, possible future work and testing for continued research.

Chapter 2

Related Research and Problem Formulation

This chapter focuses on research relating to computer vision and pose estimation problems with emphasis on research related to pose ordering or image sequencing. This includes image matching, object and face pose recognition, and object manifold analysis. Furthermore, methods that combine pose information from 2D images for constructing 3D image models is of interest in this section. Researching the relation between combining 2D information for stereo matching and computer recognition was a priority. It is thought that the ability to link these methods is required for pose sequencing tasks because most research in constructing a 3D model assumes recognizing the pose of an object.

2.1 3D Image Reconstruction and Modeling

The purpose of this section is to document some of the methods used in 3D model reconstruction from 2D images. The methods for 3D object reconstruction from 2D images requires knowledge of the object's pose relative to the camera. Examples of reconstruction algorithms can be found in [8–10]. The methods have trouble matching object geometry with motion, unless *a priori* knowledge of the sequence of poses is available. This indicates reordering the image sequence to monotonically changing angled views is necessary for accurate 3D reconstruction.

2.1.1 Structure and Motion Estimation

Joshi *et al.* [11] describe a method that recovers the shape of an object using three calibrated cameras. Epipolar geometry is used to find matching frontier points between cameras in an attempt to recover the structure of the object. The motion can be predicted and tracked from the silhouette profiles once the structure is known. This method is useful when the object has very little or no surface features to distinguish between perspective views. The method would not work well for pose sequencing and struggles with objects that have similar silhouette shapes. Moreover, using motion estimation to order object poses is impossible when then the image sequence is random.

2.2 Scale Invariant Feature Transform

The scale-invariant feature transform (SIFT) will be the described in this section. SIFT has been utilized for 3D model reconstruction from 2D images, object recognition, and

image mosaicking [12]. In [13], Brown *et al.* describe a method using SIFT to find point correspondences between multiple cameras using epipolar geometry. The corresponding points between images were run through a random sample consensus algorithm (RANSAC) to eliminate outliers. The maximum number of corresponding points between images represents an image match. A sparse 3D model is constructed from the point correspondences using epipolar geometry. This is just one example of a method that has appeared using SIFT. Other research includes [14] which uses PCA as a local image descriptor.

The first research was presented by Lowe [15] and has been referenced by many and has been the foundation for many other image matching algorithms. Results for the SIFT implementation can be seen in Chapter 4. The main steps for computing SIFT is outlined below. The steps include:

1. Computation of scale-space
2. Detection of scale-space extrema
3. Accurate keypoint localization
4. Eliminating edge responses
5. Orientation assignment
6. Local image descriptor
7. Image descriptor representation
8. Descriptor Matching

For brevity, not all steps will be described in detail, but only the most important steps from Lowe's first paper [15].

2.2.1 Computation of Scale Space

The scale space of an image is defined as:

$$L(x, y, \sigma) = G(x, y, \sigma) * I(x, y) \tag{2.1}$$

Where G is a Gaussian filter and I is the input image. The difference of Gaussians (DoG) is then calculated by:

$$D(x, y, \sigma) = L(x, y, k\sigma) - L(x, y, \sigma) \tag{2.2}$$

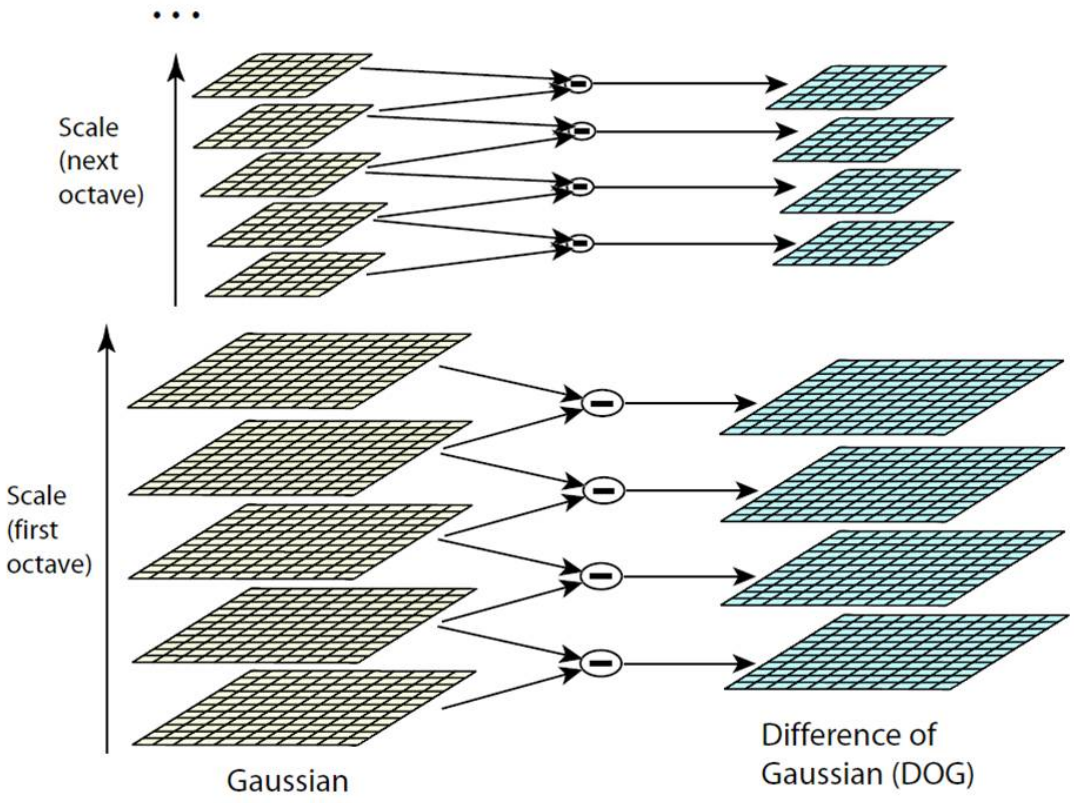

Figure 2.1: This figure shows the difference of Gaussian method used to find scale space extrema. This image was taken from [15]

Where k is a multiplicative factor. After a sufficient number of scales has been found, the scale that corresponds to 2σ is downsampled by 2 and the DoG calculation is computed for that image. An example of an efficient method for calculating DoG of scale space extrema can be see in Figure 2.1

2.2.2 Local Image Descriptor

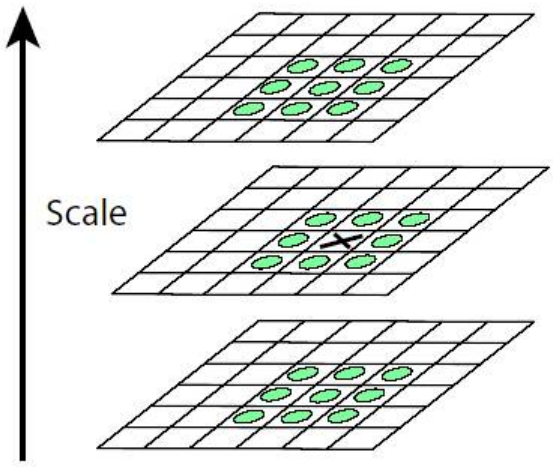

Figure 2.2: Illustation of computing local extrema

At each frame in scale-space, each point is compared to the eight nearest neighbors and then compared to the nine nearest neighbors in the scales above and below. A graphical example of this can be seen in Figure 2.2. If any of these are greater than or less than that of the point in question then that point is not a local extrema.

Removal of edge dependent image descriptors is necessary for accurate local descriptors at different scales because of shadow illumination differences. This is accomplished by first evaluating the eigenvalues of the Hessian matrix H from computing Trace (H) and Det (H) seen in equation 2.3 of the DoG images.

$$H = \begin{bmatrix} D_{xx} & D_{xy} \\ D_{xy} & D_{yy} \end{bmatrix} \tag{2.3}$$

$$\frac{\text{Trace}\,(H)^2}{\text{Det}\,(H)} < \frac{(r+1)^2}{r} \tag{2.4}$$

From equation 2.4, if r is below a certain threshold, eliminate the local extrema, corresponding to the point calculated from equation 2.3.

The remaining image pixel locations are scale invariant keypoints, used for image matching and point correspondences between images. A nearest neighbor algorithm is generally used to find point correspondences between images for recognition and matching. The SIFT method was implemented for sequencing by finding the greatest number of matched keypoints. The results can be seen in Section 4.4.

2.3 Object Recognition

This section discusses recognition methods used for computer vision that take into account varying pose angle views. These methods concentrate on proper feature space representation to include the randomness of an object view angle presented in an image. The methods of [16–18] propose dimensionality reduction to approximate the image data by creating a database for matching. The research of are a couple of the first applications of PCA to computer vision. The methods of [17–19], use a PCA reduced space manifold for matching image sequences. Laplacian eigenmaps is a more recently developed method used for transforming a reduced space manifold into clusters for classification. Some results using Laplacian eigenmaps for image ordering can be seen in Section 4.3.

2.3.1 Recognition and Varying Pose

The method of Murase *et al.* [17] uses PCA to find image features and to reduce the amount of image data for storage. This is a supervised learning method that attempts to classify objects with varying pose. To achieve this two feature spaces are needed. One is the universal object eigenspace and the other is the object pose eigenspace. The image data used for the object pose space contains many objects at monotonically changing view angles. The illumination angle is controlled by a machine, but varies with object pose. The data used for the universal eigenspace is composed of all objects and pose data. Classification starts by finding the object in universal object eigenspace using minimum distance. The pose is found in a similar manner using the pose space. This method is similar to the proposed method for this thesis. The main difference is this thesis uses a pose manifold in eigenspace for unsupervised object pose sequencing. The sequencing is used to find the position of the current camera view to that of the next view.

Moghaddam and Pentland [18] describe a search method using a large facial image database in reduced feature space to find the closest match to the input face. Preprocessing is done to the facial image in order to obtain consistency throughout the datasets for comparison. The preprocessing consists of face flattening and centering. The principal component projections are computed for dimensionality reduction and feature extraction of the facial images. The search is conducted by minimizing the distance from feature space metric (DFFS), which is the euclidean distance in the eigenface space. The pose angle is identified using a training set of faces at varying poses, then the face is matched to the face of that pose similar to the method of [17]. The differences are the preprocessing steps and the use of templates in [16, 18] to select key facial features for frontal face

recognition. It is important to note that this thesis does not use templates for key feature selection for tracking. More recent research [2, 13, 14], addresses object recognition at various poses using SIFT rather than PCA or a combination seen in [3]. These algorithms do not address the issue of sequencing the pose order of multiple images.

2.3.2 Laplacian Eigenmaps

Laplacian eigenmaps is a new field of research in machine learning, computer vision and recognition. It is an unsupervised method used for clustering. Laplacian eigenmaps are applied to a higher dimensional manifold to reduce the space for clustering in a lower dimensional space.

$$W_{ij} = \exp\left(-\frac{\|\mathbf{x}_j - \mathbf{x}_i\|}{t}\right) \tag{2.5}$$

The process begins with manifold $X = [\mathbf{x}_i \dots \mathbf{x}_k]$ with k being the number of vectorized images in X. A weight matrix W_{ij} is computed using the heat kernel given in equation 2.5. W_{ij} is computed from when $\mathbf{x}_i$ and $\mathbf{x}_j$, is an edge, or nearest neighbor, otherwise a zero is placed in W_{ij} in the corresponding matrix location. The process is repeated until all points in the manifold have been visited. Two parameters must be chosen for the weight map:

1. The value of t.

2. The number of edges to be used in the computation.

$$L\mathbf{y} = \lambda D\mathbf{y} \tag{2.6}$$

The Laplacian is defined as, $L = D - W$ where D is a diagonal weight matrix calculated from equation 2.5, such that $D_{ii} = \sum_j W_{ij}$. The eigenmap is computed by solving the generalized eigenvalue problem in equation 2.6.

From equation 2.6, the eigenvalue with the lowest value corresponding to the matrix of eigenvectors **y** is the solution to the Laplacian matrix. The rank of the Laplacian matrix indicates the number of eigenvectors yielding a trivial solution. For this reason, care must be taken when selecting the eigenmaps.

2.3.3 Manifold Learning

Constrained manifold learning has been used to estimate camera pose, generate matched animations, and to match human lip movements. An example for manifold matching from [19] can be seen in Figure 2.3.

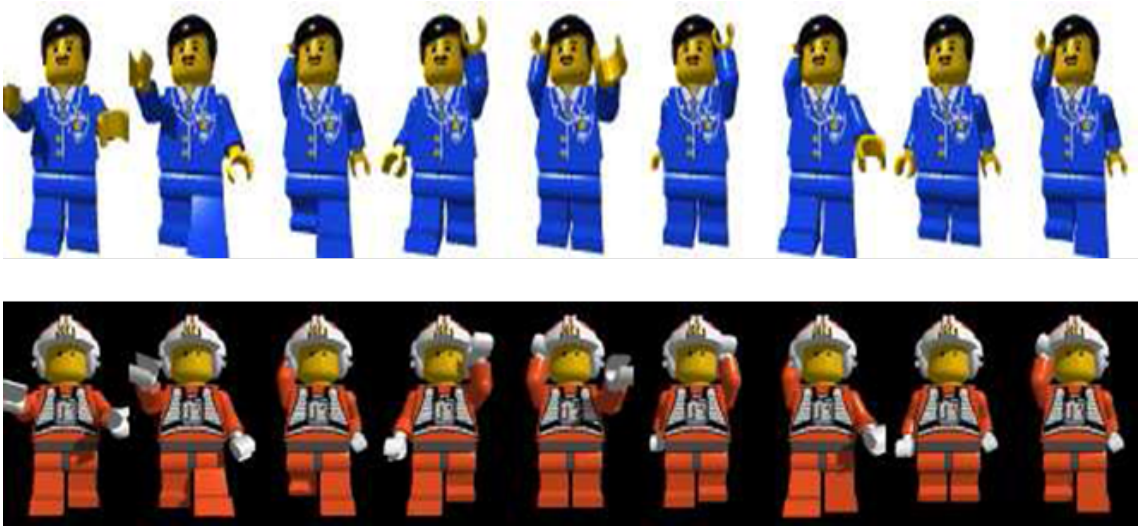

Figure 2.3: This figure shows an example of matching animations of a toy figure

This is a non-iterative method using the concept of diffeomorphism to generate a map between two manifolds $x \in X$ and $y \in Y$. In mathematics, diffeomorphism is an invertible function that maps one differentable manifold to another. In this case, the

manifolds are generated in PCA space from images x and y, such that X and Y are the manifold spaces. Learning manifold maps in [19] is based on computing a local manifold smoothness. Manifold smoothness in PCA space is used in this thesis as well. Chapter 3 will discuss this in more detail.

2.3.4 Image Feature Distributions

One method described in [14, 20] uses the earth movers distance (EMD) to match images from a database. The EMD operates on image feature distributions and is described as the amount of work needed to match one histogram of image features x_i to another y_j. This method is useful for matching overall image content, such as matching similar background scenes and characters. However it does not discriminate fine spatial features to capture and order the motion in the images. This is due to the loss of spacial information when binning pixels into a histogram. Furthermore, histogram matching needs high variability in the pixel distributions not considering the variation of an entire data set.

2.4 PCA Solution for Pose Ordering

This section is intended to explain the problem of pose ordering using PCA. A problem description has been formulated to explain why PCA is chosen as a feature space and the benefits that PCA can offer. The benefits provided will expose it's drawbacks for certain applications.

2.4.1 PCA Description

The problem for ordering random object poses is viewed as a problem in pose recognition. This problem is primarily solved using principal component analysis (PCA) because of it's simplicity. Moreover, computing PCA on sequences of object poses produces distinct geometry in eigenspace. This occurs because of the properties and assumptions of PCA:

1. Dimensionality reduction
2. Linear combination of feature components
3. Gaussian distributed feature components
4. Orthogonality of feature components
5. Linear transformation

PCA offers dimensionality reduction for developing large databases of training data for recognition. Dimensionality is reduced by minimizing the mean square error over the dataset. Feature selection is performed by choosing a linear combination from the data containing the maximum variance. The maximum variance across the data set satisfies the minimum mean square error criteria for embedding the data in a reduced space. This is an important aspect to any pattern recognition problem. The eigenvectors and eigenvalues of the autocorrelation matrix of the data correspond to the orthogonal basis function and the decorrelated variance,respectively. The features are a result from the minimization of the error of the projection space to the data known as the eigenspace. The number of components is the rank of the autocorrelation matrix.

The criteria for dimensionality reduction using PCA assumes the data is Gaussian distributed with an unbiased mean and variance. PCA is an optimal embedding technique for Gaussian distributed data, because it captures the mean and variance as defined by a Gaussian probability distribution. Multimodal data does not follow the know equations for the mean and variance. This breaks the assumption of an optimal embedding space for minimizing the mean square error with maximum variance. Important data is now lost making it impossible for correct classification. However, for image processing purposes used in this thesis, the manifold from the assumed Gaussian distribution is of interest. This implies that PCA is optimal for data embedding and comparison.

The optimal embedding space, as stated previously, are the eigenvectors of the auto-correlation matrix of the image data set. Eigenvectors are known for the property of being orthogonal to each other. Having an orthogonal space means that each basis dimension is uncorrelated to the another. This is characteristic of the diagonalization of the autocorrelation matrix. This is another source of data loss because linear mixtures may exist within a single principal component. However, the property is desirable when the objective is to indiscriminately extract all spatial variant features across the image data set. It comes to be a problem when specific image features are desired other than the maximum variance. This thesis shows that neither classification nor clustering is a desired technique for image pose ordering. Rather the pose ordering method is seen as a process of sequencing images by the arrangement of the PCA representation of the unordered image set. This offers a solution to ordering under the condition that it is a scatter of points producing a structured manifold in eigenspace.

The linearity of PCA is a highly desired characteristic for ordering random object poses. PCA is the result of the linear combination of the variance and cross-variance

of each pixel over an entire set of images, is independent of the order of the images. This implies the input order of the image sequence does not dictate the structure of the manifold and the multidimensional eigenspace is the same regardless of the random order of images.

2.4.2 PCA for Pose Recognition

The idea of using PCA for pose ordering comes from the previous work done in supervised pose recognition (see Section 2). This work [17] shows results of multidimensional manifolds in eigenspace for each object at different poses and different illumination. Each point in eigenspace represents an object pose. As the manifold trajectory is traced to each image the pose angle changes. The minimum distance to the object space and the minimum distance to the pose space is the solution for recognition of the object and pose view respectively. The shape and the resolution of the manifold will dictate the ordering results. Increasing the number of image views with varying illumination would achieve a more accurate pose sequencing. If not, a more sophisticated algorithm will be needed for high pose ordering accuracy. This will be seen later within the results in Chapter 4.

Chapter 3

Theoretical Development of the Pose Ordering Algorithm

3.1 Principal Component Analysis

The rational for using Principal Component Analysis (PCA) has already been provided in Section 2.4.1. The next section will help to explain the how PCA is applied to a sequence of images for the purpose of ordering view-angles. Furthermore, this section will show image examples and explain eigenposes. These are the basis functions used for computing the geometrical configuration of a set of random object poses. A treatment of PCA can be found in [21].

3.1.1 Mathematical Description of Proposed Method

Each image $\mathbf{x}_i$ of size $M \times N$ in the randomly captured sequence is formed into an $MN \times 1$ vector. This is done for the entire set of images and concatenated into a matrix

$\mathbf{X} = [\mathbf{x}_1, \ldots, \mathbf{x}_K]$ of random object poses. Normalization is not done across the image set. This way, illumination and shadows are preserved as these are seen as features for ordering poses. The next step is to calculate the eigenspace of the random set. The eigenspace basis matrix $\mathbf{E}$ is composed of the L largest corresponding eigenvalues for some L. The square matrix $\mathbf{Q} = \mathbf{X}\mathbf{X}^T$ is computed and singular value decomposition is done such that:

$$\mathbf{Q} = \mathbf{E}^T \Lambda \mathbf{E} \tag{3.1}$$

Where Λ is the diagonal matrix of eigenvalues.

$$\mathbf{g}(\mathbf{x}_i) = \mathbf{x}_i^T \mathbf{E} \tag{3.2}$$

The projection $\mathbf{g}(\mathbf{x}_i)$, of size $L \times 1$, of the image onto the eigenspace is then calculated and used as the feature space.

3.1.2 "Eigenpose" Analysis

The eigenvectors were plotted to visualize the dominant features for some test objects. These plots can be seen in Figures 3.1 and 3.2. The term "eigenposes" was taken from the term "eigenfaces" in [18]. The first ten principal components eigenvector images are computed using:

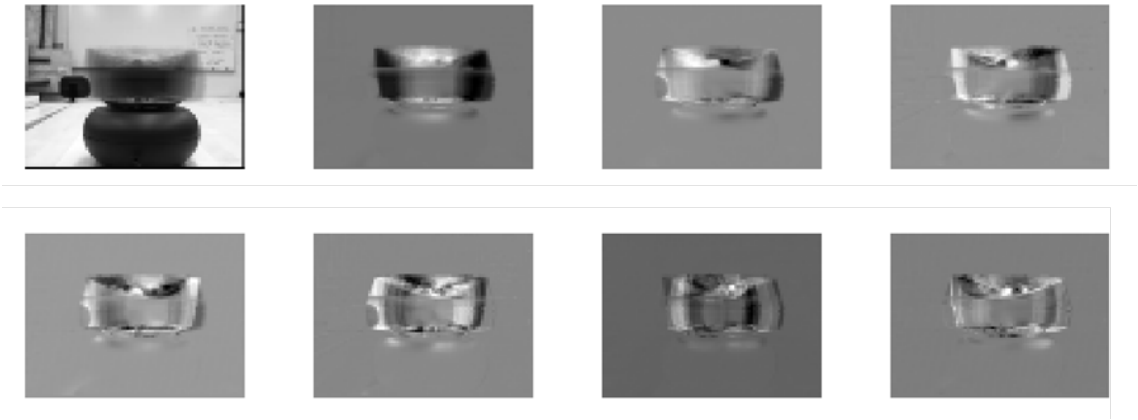

Figure 3.1: Eigenvectors for an object with less details

Figure 3.2: Eigenvectors for an object with more details

Where $\mathbf{e}_i$ is the unit eigenvector found in the i^{th} column of $\mathbf{E}$ and λ_i is the i^{th} diagonal component of Λ seen in equation 3.1. After this is done, the vector must be rearranged into an image given width and height dimensions.

$$\text{Eigenpose}_i = \sqrt{\lambda_i}\mathbf{e}_i \tag{3.3}$$

The principal component eigenvalues associated with the eigenposes for each the tape and

truck images can be seen in Figure 3.3 plotted on a logarithmic scale. It can be noted that the eigenvalues drop off faster in the truck images than in the tape images.

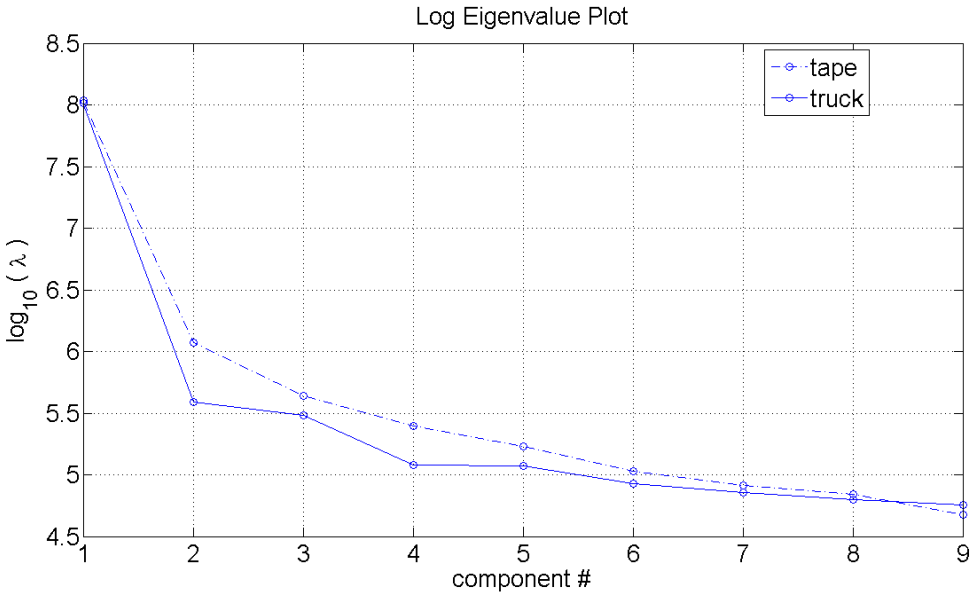

Figure 3.3: Base ten logarithm of the eigenvalues associated with the first nine eigenvectors seen in Figures 3.1 and 3.2

The number of principal components utilized can be determined from equation 3.4 seen in [17].

$$I = \frac{\sum_i^L \lambda_i}{\sum_i^{MN} \lambda_i} \tag{3.4}$$

The output, I, is the fractional amount of information that is explained by the variance in the image set. The information measure should be close to one. For each object tested, I was computed to represent 99% of the information from the variance and can be seen in Table 3.1.

Object	PCs	Information
Tape dispenser	4	0.9914
Truck	3	0.9916
Airplane	5	0.9917
Stapler	3	0.9936
House	16	0.9901
Cylinder	2	0.9910
Battery	1	0.9937

Table 3.1: Information measurement for each object tested

Table 3.1 shows the number of principal components needed to represent 99% of the information from the variance. Section 4.2.3 will show experimental results for the amount of information needed.

3.2 Object Pose Ordering

The proposed approach for ordering images is an iterative process. Let S_j and Θ_j be the set of unordered and ordered images at iteration j, respectively. To begin, S_0 is the entire set of unordered images and Θ_0 is the empty set of ordered images. At iteration $j = 1$, a randomly chosen image is labeled $\mathbf{x}_1$ and moved from S_0 to Θ_0, yielding S_1 and Θ_1. For $j \geq 2$ an image $\mathbf{x}_j$ is moved from S_{j-1} to Θ_{j-1} such that:

$$\mathbf{x}_j = \underset{\mathbf{x} \in S_{j-1}}{\operatorname{argmin}} \left(\left\| \mathbf{g}\left(\mathbf{x}_{j-1}\right) - \mathbf{g}\left(\mathbf{x}\right) \right\| \right) \tag{3.5}$$

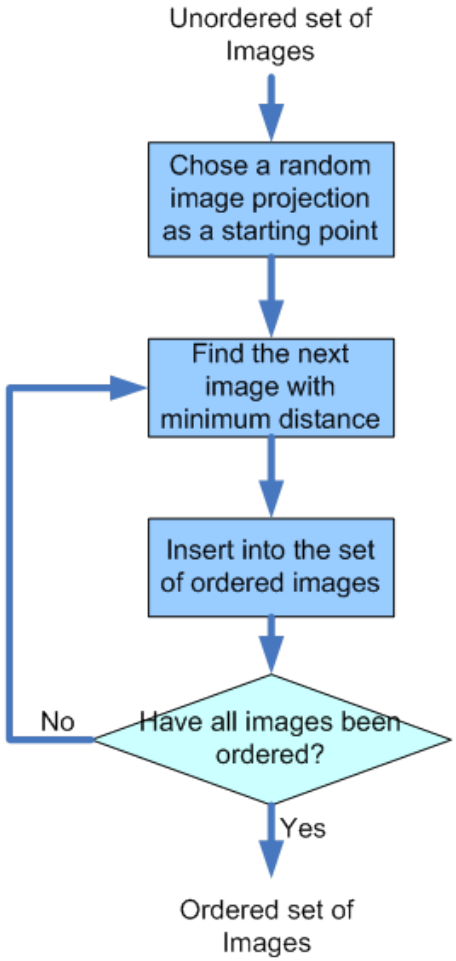

Figure 3.4: Block diagram of the single camera ordering algorithm implemented

Thus, the ordering algorithm picks from the unordered set, the image closest to the last ordered image in eigenspace. The diagram in Figure 3.4 shows the algorithm for single camera ordering. Once the images have been ordered using the minimum separation, a confidence measure is computed using local curvature along the trajectory (called the object manifold) of the ordered images in eigenspace.

Let $\mathbf{ds}_j$ be the vector:

$$\mathbf{ds}_j = \mathbf{g}\left(\mathbf{x}_j\right) - \mathbf{g}\left(\mathbf{x}_{j-1}\right) \tag{3.6}$$

The cosine of the angle between the vectors is the correlation coefficient:

$$\cos\left(\theta_j\right) = \frac{\mathbf{ds}_j^T \mathbf{ds}_{j-1}}{\left\|\mathbf{ds}_j\right\| \left\|\mathbf{ds}_{j-1}\right\|} \tag{3.7}$$

The difference between vectors is then computed by subtracting the two vectors. The difference equation is an approximation to the second order derivative for curvature:

$$\kappa_j = \sqrt{\left(\mathbf{ds}_{j-1} - \mathbf{ds}_j\right)^T \left(\mathbf{ds}_{j-1} - \mathbf{ds}_j\right)} \tag{3.8}$$

The confidence in ordering metric is given by:

$$c_j = \kappa_j \left(1 - \cos\left(\theta_j\right)\right) \tag{3.9}$$

3.2.1 PCA Based Distance Metrics

Other PCA based distance metrics were tested for the use with pose ordering [22]. For these equations $\mathbf{g}_i(\mathbf{x})$ represents each principal element of the projection transformation from equation 3.2.

- Euclidean distance:

$$d(\mathbf{g}(\mathbf{x}_{j-1}), \mathbf{g}(\mathbf{x})) = \sqrt{\sum_i \left(\mathbf{g}_i(\mathbf{x}_{j-1}) - \mathbf{g}_i(\mathbf{x})\right)^2} \tag{3.10}$$

- Angle based distance:

$$d(\mathbf{g}(\mathbf{x}_{j-1}), \mathbf{g}(\mathbf{x})) = -\cos(\mathbf{g}(\mathbf{x}_{j-1}), \mathbf{g}(\mathbf{x})) \tag{3.11}$$

$$= \frac{\sum_i \mathbf{g}_i(\mathbf{x}_{j-1}) \mathbf{g}_i(\mathbf{x})}{\sum_i \mathbf{g}_i(\mathbf{x}_{j-1})^2 \sum_i \mathbf{g}_i(\mathbf{x})^2} \tag{3.12}$$

- Mahalanobis distance:

$$d(\mathbf{g}(\mathbf{x}_{j-1}), \mathbf{g}(\mathbf{x})) = \sum_i z_i \mathbf{g}_i(\mathbf{x}_{j-1}) \mathbf{g}_i(\mathbf{x}) \tag{3.13}$$

  where $z_i = 1/\lambda_i$

- Manhattan distance:

$$d(\mathbf{g}(\mathbf{x}_{j-1}), \mathbf{g}(\mathbf{x})) = \sum_i z_i \left| \mathbf{g}_i(\mathbf{x}_{j-1}) - \mathbf{g}_i(\mathbf{x}) \right| \tag{3.14}$$

  where $z_i = 1/\lambda_i$

The distance metric that produced the best results was the eucleadian distance. This is because it takes into account the geometrical separation and preserves the significance of the principal component transformation. The other metric either normalize the significance of each component or normalize the distance, which makes it difficult to compare each image pose angle.

3.2.2 Confidence Metric

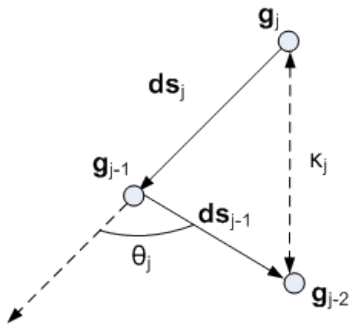

Figure 3.5: The vector representation of the confidence measure

The confidence metric c_j attempts to use a combination of three local image projections to measure the alignment and the curvature. The alignment is equivalent to the congruence coefficient across three images and is equal to zero when they are in a straight line. The curvature acts as a weight across the combination of the three images. A low confidence measure indicates the images are changing slowly and pose classification is more accurate in this region and a high measure of confidence means the images are changing erratically. For this confidence measure, a low value is desirable to indicate correct ordering. The vector representation for these can be seen in Figure 3.5.

3.2.3 Development of the Confidence Metric

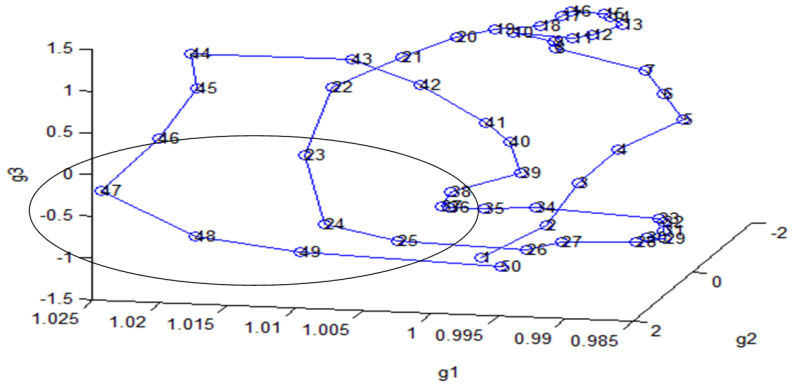

(a) Correct pose manifold trajectory

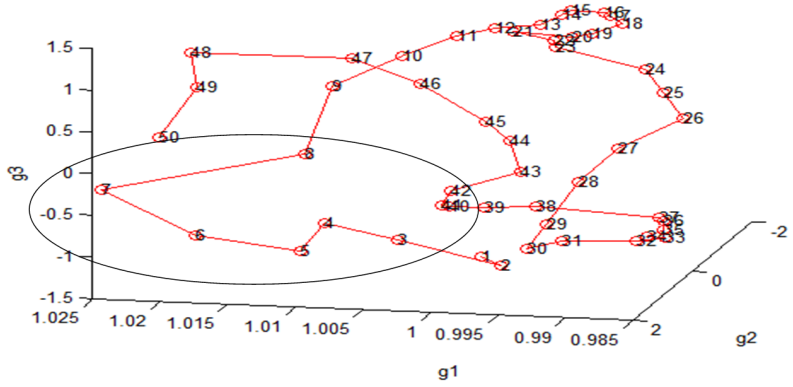

(b) Incorrect pose manifold trajectory

Figure 3.6: Comparison of the correct manifold and the incorrect manifold

The development of the confidence metric was motivated by the problem of detecting errors in ordering. A geometrical feature was chosen as a metric because of the trajectory of pose images projected onto the eigenspace seen in Figure 3.6. Figure 3.6(a) was

produced by direct computation of PCA on the order image sequence. Figure 3.6(b) was produced using the ordering algorithm seen in Figure 3.4. Differential geometry defines the trajectory of a moving particle in space to be $\gamma(t)$. This is the representation of the object manifold. Therefore, the formal definition of curvature is given as:

$$\kappa(t) = \left\| \gamma''(t) \right\| \tag{3.15}$$

For the purposes of this thesis, the difference equation of this measure is used and was given in equation 3.8.

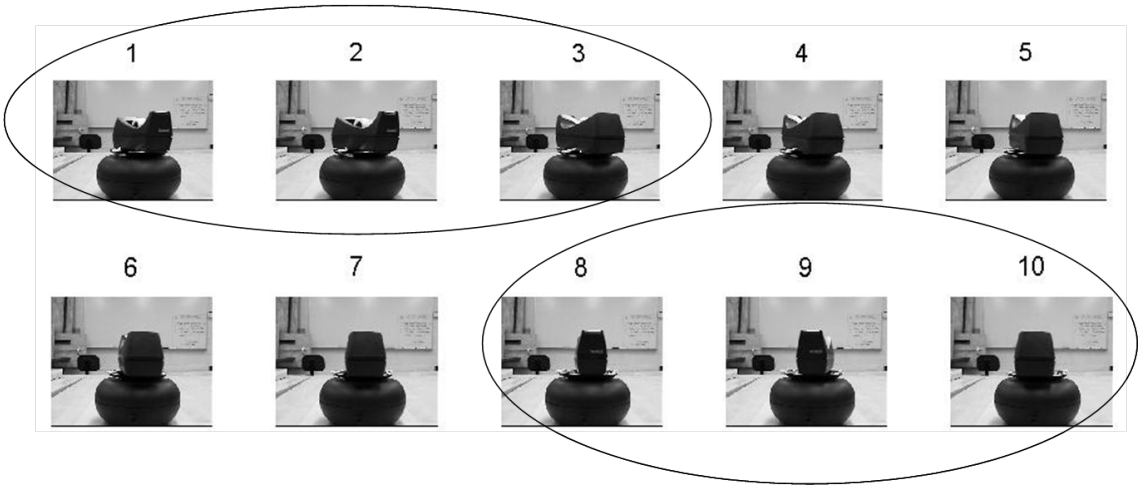

(a) Images 1-10 corresponding to the first two errors

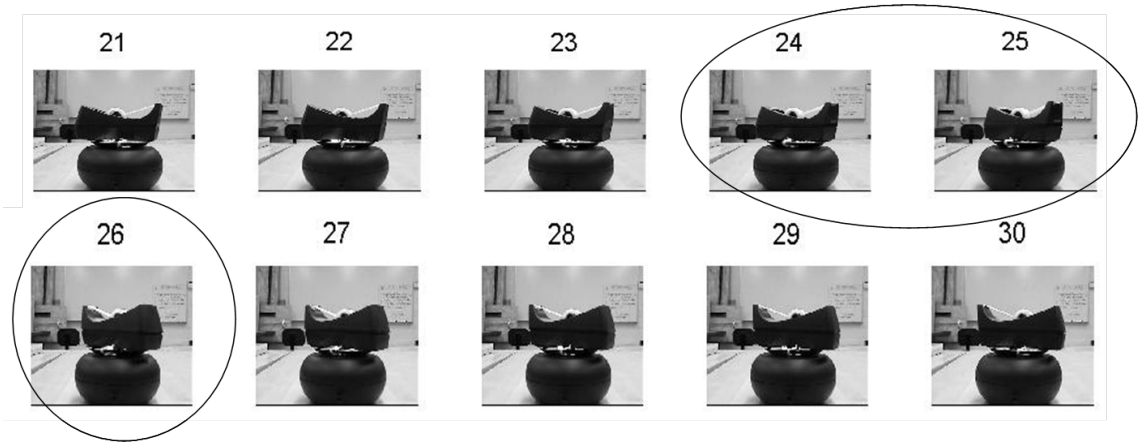

(b) Images 21-30 corresponding to the third error

Figure 3.7: Image data set observed in Figure 3.8

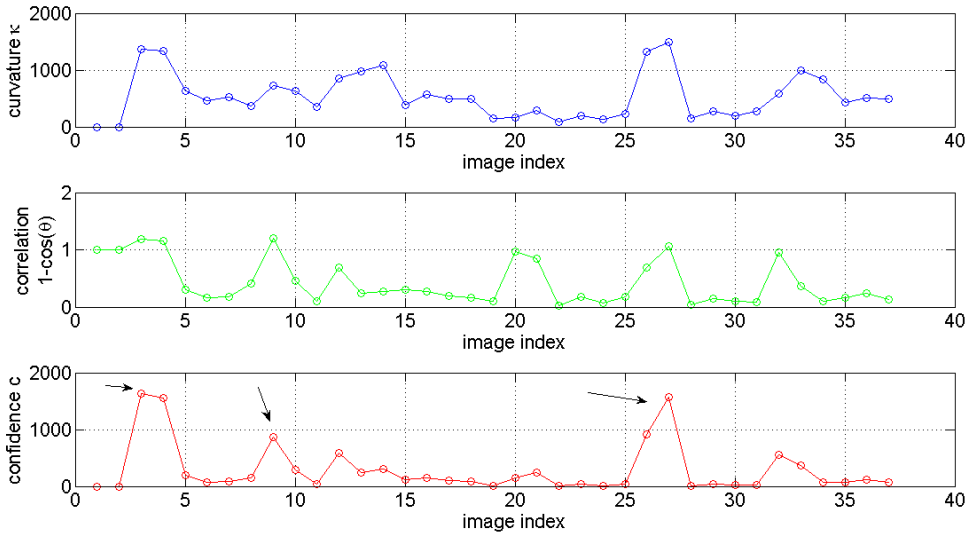

Figure 3.8: **Top:** Curvature, **Middle:** one minus correlation, **Bottom:** confidence. These were calculated after pose ordering. The arrows point out the errors observed in pose ordering

The two types of metrics chosen for ordering are curvature, κ_j, and correlation, $\cos(\theta_j)$, as described in the previous section. Plots of these metrics for a test object are shown in Figure 3.8. The single camera algorithm used to produce the results is seen in Figure 3.4. The figure is intended to show how the combination of the two metrics perform the task of recognizing errors within the single camera ordering algorithm. The errors are referenced by the arrows in Figure 3.8. The images that correspond to these errors can be seen in Figure 3.7(a) and 3.7(b). It is important to note that the confidence is calculated using three images, therefore each point represents images indices $j-2$, $j-1$, and j.

It is difficult to observe, by an untrained eye, the errors in pose ordering of Figures 3.7(b) and 3.7(a). Indeed these are 180° apart in view-angle because of the similarity in

the front and back views of the object.

3.3 Two Camera Ordering with Confidence

This section is intended to explain, in detail, the confidence metric utility integrated into the two camera architecture. The main idea is to use the confidence metric to correct the errors found when ordering using the minimum distance. To achieve this, a second camera has been included in the experiment. This second camera creates additional information used for the pose ordering algorithm.

3.3.1 Two Camera Configuration

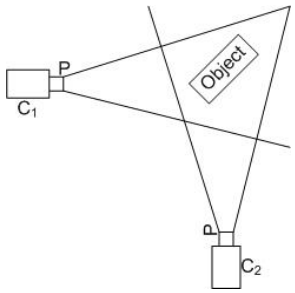

Figure 3.9: Two camera configuration used in the experiment

The two camera configuration can be seen in Figure 3.9. The two cameras are placed 90° apart in viewing angle in an attempt to gain more salient object features and eliminate the 180° errors seen in Figure 3.7, images 9 and 10. These errors are because the pose space of the object is dominated by side views. Physically the side view is larger containing more pixels and will be included in a majority of the images. This will effect the PCA

variance maximization feature extraction. Some eigenvectors were seen in Figures 3.1 and 3.2.

3.3.2 Implementation of the Confidence Metric

The single camera method is extended to the case where two synchronized cameras are available. Since the cameras are synchronized, we can compare the time indices of each camera. By independently ordering each camera's images, it can be said that if the time indices do not match, then an error in ordering has occurred. The difficulty lies in determining automatically which camera view is more likely to have incorrectly ordered the images. This is done by comparing the confidence c_j developed in the previous section and time indices of each camera to determined if an error has occurred and which camera has the lower confidence of error. If $c_j^{camera1} > c_j^{camera2}$ then camera two is chosen for the next view and vice versa. A block diagram for the algorithm described can be seen in Figure 3.10.

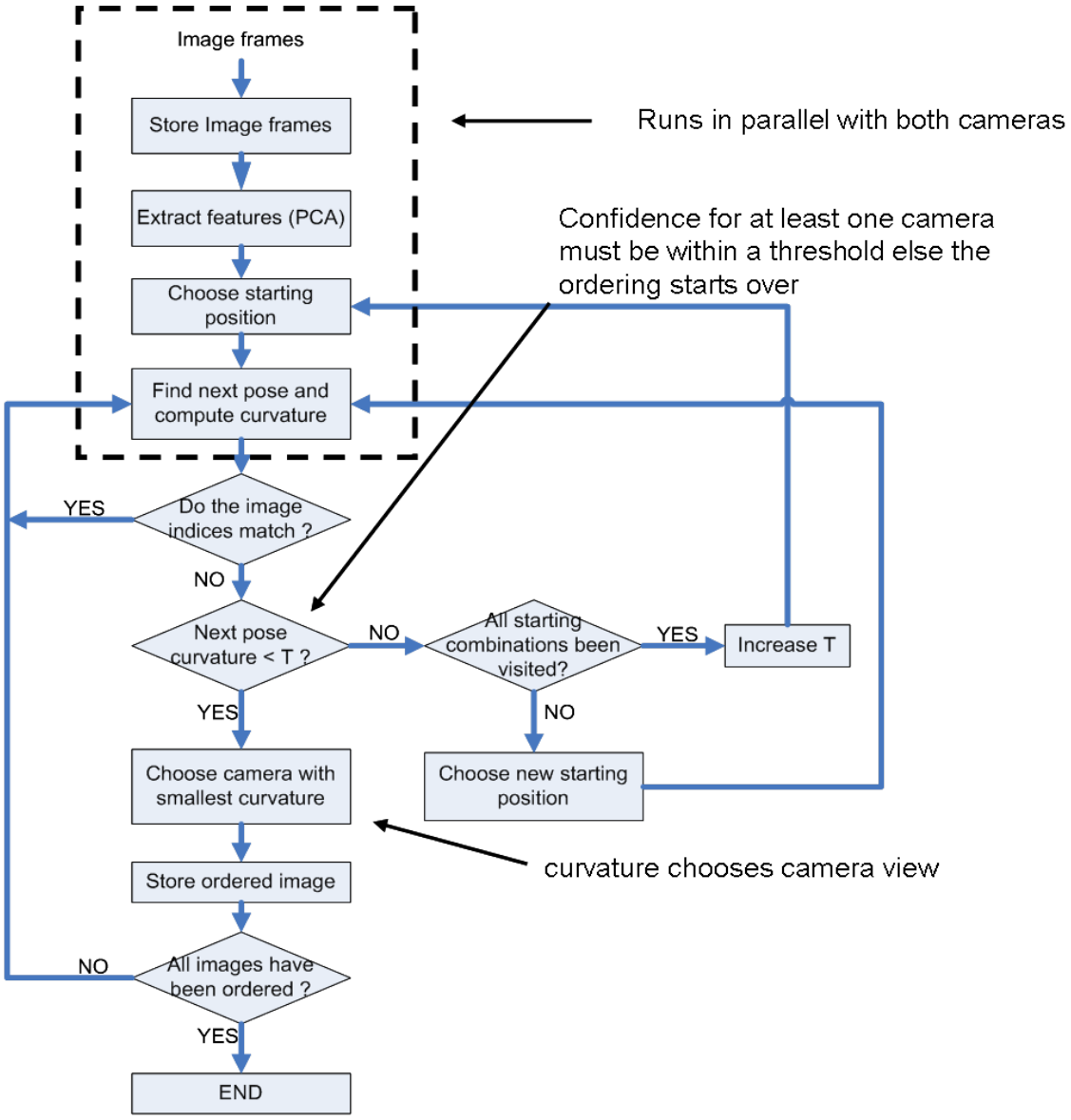

Figure 3.10: Block diagram for the two camera ordering algorithm

3.3.3 Confidence Thresholding

A large confidence metric is intended to exploit problem areas for pose ordering in the object manifold. What happens when both confidence values are significantly large? Consider a value T as a threshold to detect outliers in the confidence values. Any confidence value greater than T is an outlier. The ordering method is designed such that: if $c_j^{camera_1} > c_j^{camera_2}$ and $c_j^{camera_2} > T$, then reject the hypothesis that camera two is the correct next pose. This is because the confidence in ordering is not high.

$$\mu = \frac{1}{N}\sum_j c_j^{camera_k} \tag{3.16}$$

and the standard deviation by:

$$\sigma = \left(\frac{1}{N-1}\sum_j \left(c_j^{camera_k} - \mu\right)^2\right)^{1/2} \tag{3.17}$$

and N is the number of confidence values (number of images $-$ 2). This can be seen in Figure 3.11.

$$T = \mu + \sigma \tag{3.18}$$

To initialize the confidence metric threshold, all confidence values are computed for a single image. Next, a threshold is chosen from the statistics of the confidence distribution. This can be seen in equation 3.18, where the mean is calculated by:

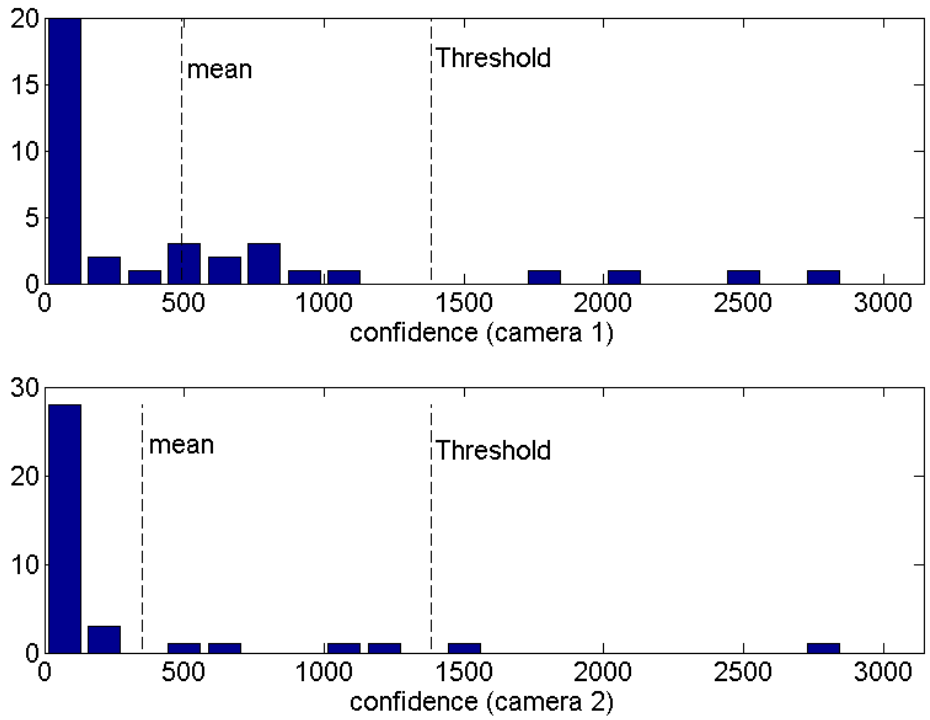

Figure 3.11: Histogram of the confidence values for the two cameras. The threshold and mean are shown as dotted lines.

If the camera hypothesis for the confidence values is rejected, then the threshold is increased by a factor (10% is used in the results). By increasing the threshold, the method will eventually converge to a pose ordering solution. This step can be seen in the block diagram of the algorithm in Figure 3.10

Chapter 4

Results

4.1 Procedure

The results were obtained from videos taken of many objects on a turntable. The first test was pose sequencing with a single camera, and the second test was pose sequencing with two synchronized cameras. Please refer to Section 3.3.1 for two camera configuration. The video sequence was scrambled in MATLAB using a uniform random number generator. The known video sequence is used to help with assessing the results of ordering. The random number set is used to produce an equal distribution for the full rotation of the object. This means that no views are repeated and if a histogram of pose angle was created, then there would be only one count per bin. A set of images that includes a full rotation of the object ensures that the first and last images are connected in eigenspace. It also makes error counting and validation of the ordering simpler. The video frame rate is 16 frames/sec and the number of poses in a set varies from 30 to 37 depending on the random number seed. The images are downsampled by a factor of four to a size of 80×60.

This is done to accommodate the large size of the covariance matrix. The formulation of the covariance matrix for PCA is not normalized by illumination. It is thought that illumination is a feature for recognition of objects and scenes used by human vision.

The error rate for object ordering is calculated manually by visual inspection of the images and counting the number of incorrectly sequenced images. By definition, an error occurs if the next pose does not correspond to the current pose for the set of images. Error rate is calculated for the entire set by summing the total number of errors and dividing by the number of images in the set.

Object	Single Camera	Two Cameras	Gain
Tape dispenser	17.0%	0.9%	16.1%
Stapler	9.1%	0.3%	8.8%
Truck	6.7%	0.3%	6.4%
House	3.0%	0.9%	2.1%
Airplane	1.5%	0.3%	1.2%
Cylinder	0.6%	0.0%	0.6%
Battery	0.3%	0.0%	0.3%

Table 4.1: Error Rate of Ordering Various Objects

Objects without distinct features have failed to order properly in the single camera case because of the similarity of views. These objects without saliency are referred to in Table 4.1 as the tape dispenser and the truck. For these types of objects, the recognition errors generally misclassify the front and back views corresponding to 180° of rotation.

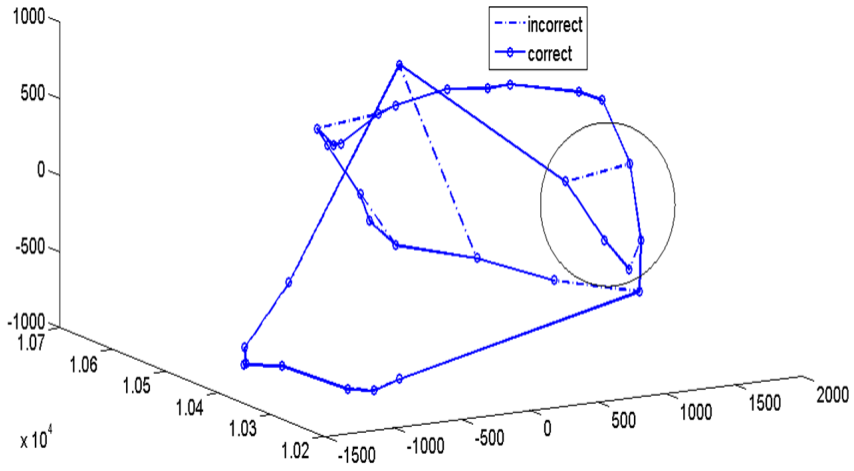

Figure 4.1: Example of errors in the pose manifold reconstruction

Most of the errors occur where the manifold begins to wrap around itself and become tangled. This can be shown in Figure 4.1, where the circled region represents the problem area when the next angle-view is not the minimum distance. The dotted line shows the errors for ordering with a single camera. The solid line in Figure 4.1 shows the correct manifold reconstruction using two cameras with the confidence metric.

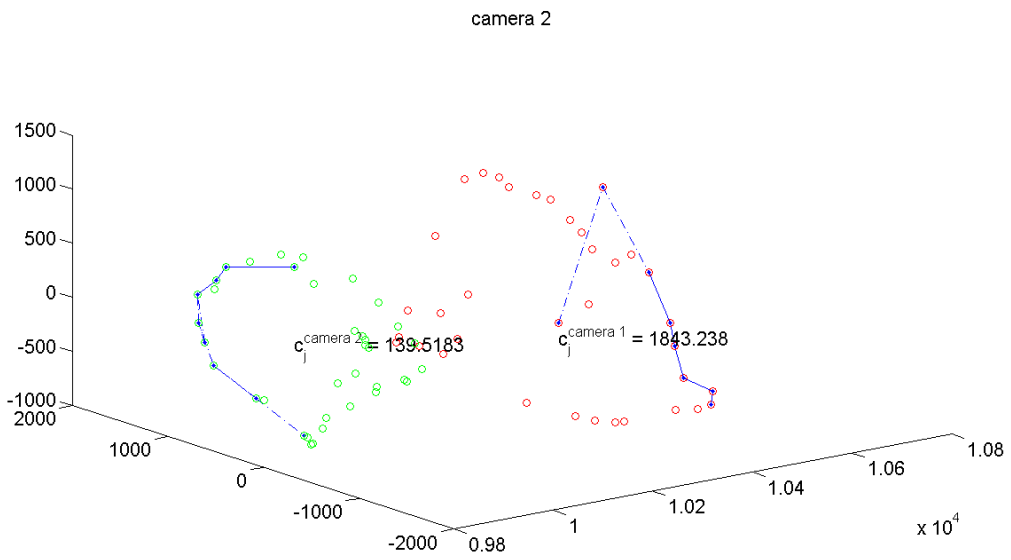

Figure 4.2: This figure plots both manifolds from camera 1 and camera 2, and shows the errors in dotted lines and correctly ordered in the solid lines. The confidence value is also printed for the last manifold connection made

A depiction of how the confidence measure helps to select the correct camera for viewing can be seen in Figure 4.2. The figure shows the camera whose manifold is chosen contains the section that is the most flat and is the minimum distance across images. In the example in Figure 4.2, camera one has made an error and camera two is chosen as the correct order.

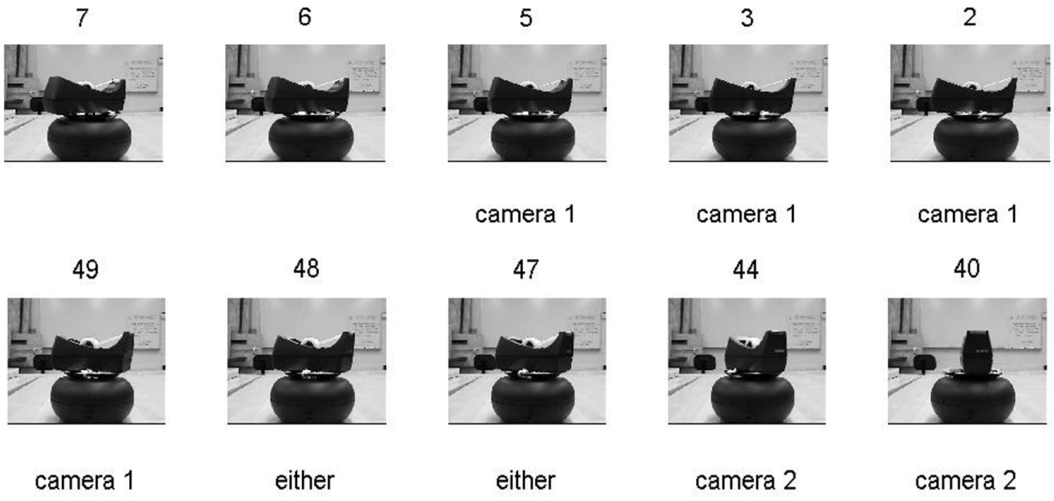

Figure 4.3: Results for two camera ordering

Figure 4.3 shows an example of the confidence selecting between camera one and camera two for front and side views of the tape dispenser. The images displayed in Figure 4.3 are seen from the perspective of camera one. As the front view appears, camera one has trouble with recognizing the next pose, therefore, it switches to camera two.

4.2 Pose Ordering Error Analysis

Trial #	Single Camera	Two Cameras
1	5	2
2	4	0
3	7	0
4	5	0
5	6	0
6	7	0
7	5	1
8	7	0
9	5	0
10	5	0
Avg	5.6	0.3
Var	1.04	0.41
Avg error	17.0%	0.9%

Table 4.2: Number of errors for the tape dispenser

In trial seven the single error can be classified as a depth perception error, and can be seen in figure (input 2 camera results)

Trial #	Single Camera	Two Cameras
1	2	0
2	5	1
3	2	0
4	0	0
5	2	0
6	3	0
7	2	1
8	2	0
9	3	0
10	2	0
Avg	2.3	0.1
Var	2.33	0.11
Avg error	6.7%	0.3%

Table 4.3: Number of errors for the truck

Trial #	Single Camera	Two Cameras
1	2	0
2	2	1
3	4	0
4	2	0
5	3	0
6	3	0
7	4	1
8	3	0
9	4	0
10	3	0
Avg	3.0	0.1
Var	0.6	0.09
Avg error	9.1%	0.3%

Table 4.4: Number of errors for the stapler

Trial #	Single Camera	Two Cameras
1	0	0
2	0	0
3	0	0
4	3	1
5	0	0
6	0	1
7	3	0
8	0	1
9	1	0
10	3	0
Avg	1.0	0.3
Var	1.8	0.21
Avg error	3.0%	0.9%

Table 4.5: Number of errors for the house

Trial #	Single Camera	Two Cameras
1	1	0
2	0	0
3	0	0
4	0	0
5	1	1
6	0	0
7	0	0
8	0	0
9	1	0
10	2	0
Avg	1.0	0.3
Var	1.8	0.21
Avg error	3.0%	0.9%

Table 4.6: Number of errors for the paper airplane

Trial #	Single Camera	Two Cameras
1	0	0
2	0	0
3	0	0
4	1	0
5	0	0
6	0	0
7	0	0
8	0	0
9	1	0
10	0	0
Avg	0.2	0.0
Var	0.16	0.00
Avg error	0.6%	0.0%

Table 4.7: Number of errors for the cylinder

Trial #	Single Camera	Two Cameras
1	0	0
2	0	0
3	0	0
4	0	0
5	1	0
6	0	0
7	0	0
8	0	0
9	0	0
10	0	0
Avg	0.1	0.0
Var	0.09	0.00
Avg error	0.3%	0.0%

Table 4.8: Number of errors for the battery

This section shows tables of error rates for each object tested. Table 4.1 contains a summary of all the object results, while Tables 4.2-4.8, contain results for individual trials for each object. A trial is a different randomization of poses used for each object. This includes different starting points for the algorithm and different angled-views taken from the database.

4.2.1 Single Camera

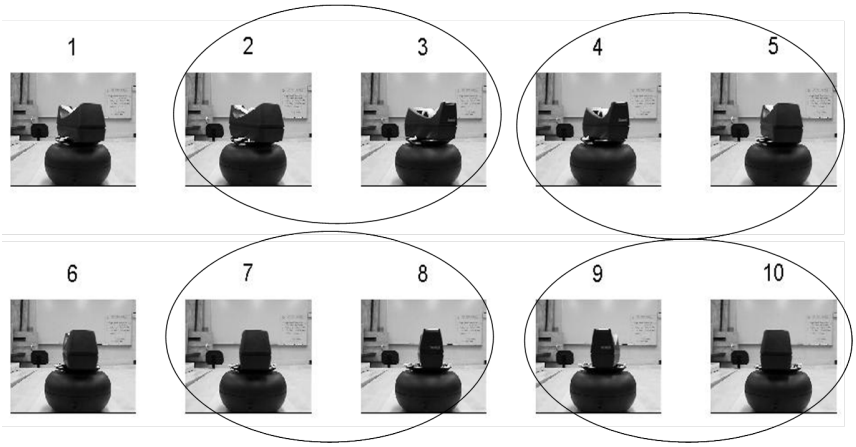

Figure 4.4: Tape dispenser images 1-10

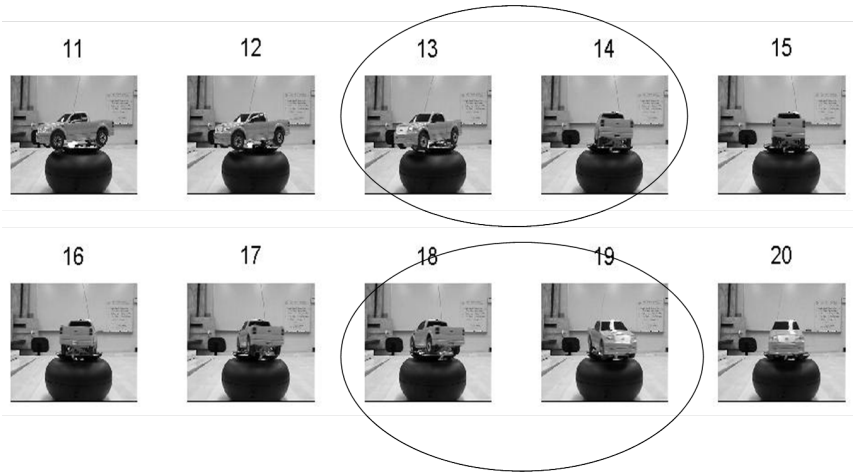

Figure 4.5: Truck images 11-20

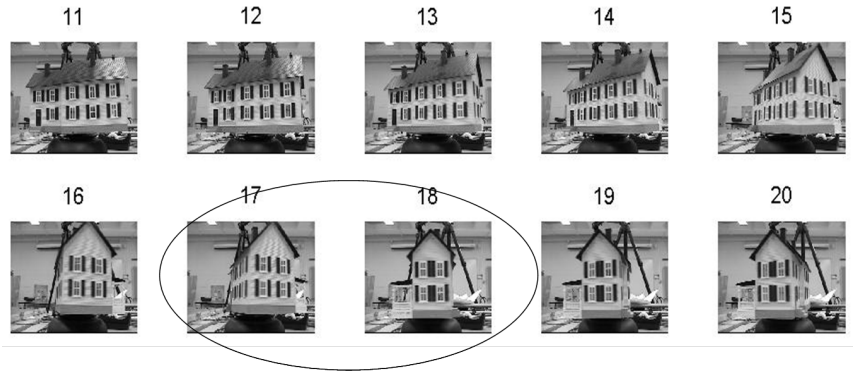

Figure 4.6: House images 11-20

This section will show image examples in the single camera ordering process. The previous section shows the errors in terms of the eigenspace representation. This section displays errors that correspond to image ordering. Figure 4.4 shows 4 errors occuring in the sequence of ten images. These errors are caused by the confusion between the front and rear views of the object. The confusion is caused by PCA dimensionality reduction and it's inability to select the required features to distinguish between these views. Some of these object views require certain details that become eliminated when using PCA. This will be shown in the reconstructed images using nine principal components. These same results can be seen in figures 4.5 and 4.6.

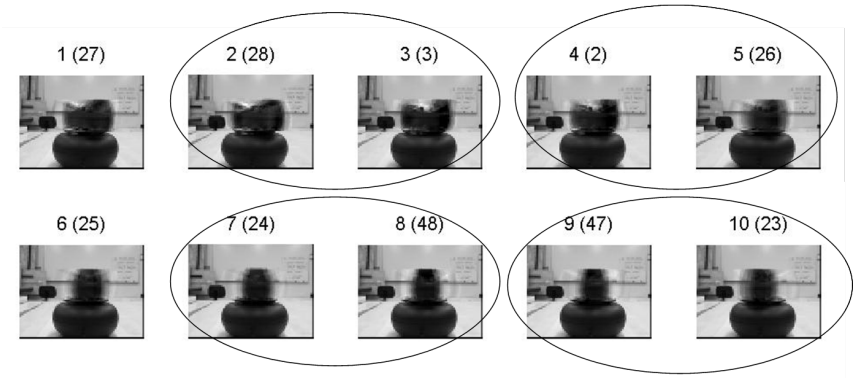

Figure 4.7: Image reconstruction using the first nine principal components for the tape dispenser images. The numbers in parenthesis represent the indices from the original video

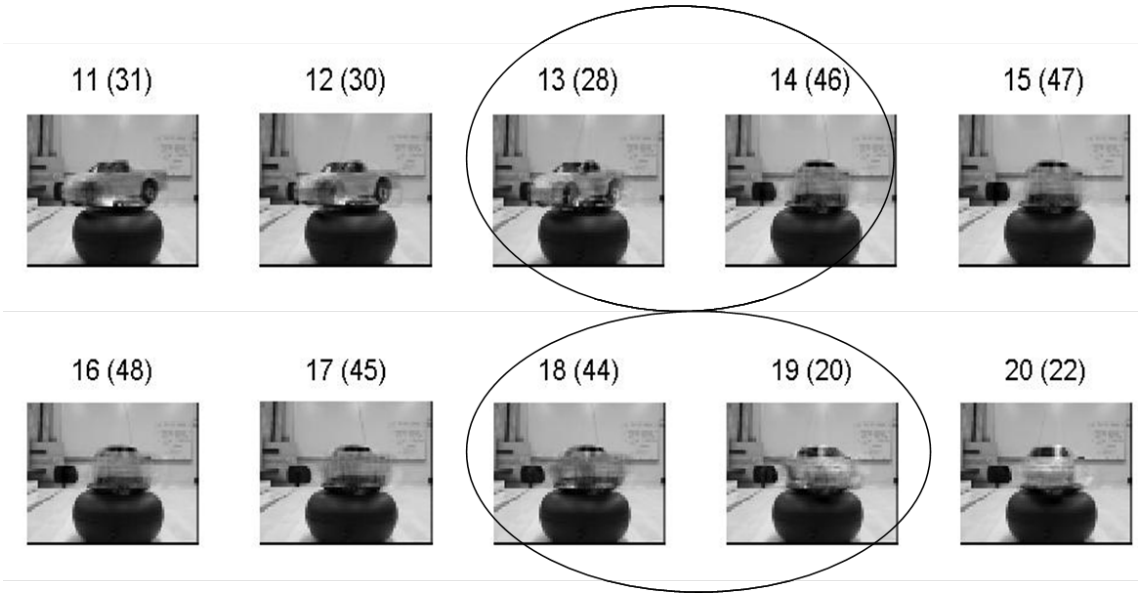

Figure 4.8: Image reconstruction using the first nine principal components for the truck images. This image can be compared to that in Figure 4.5

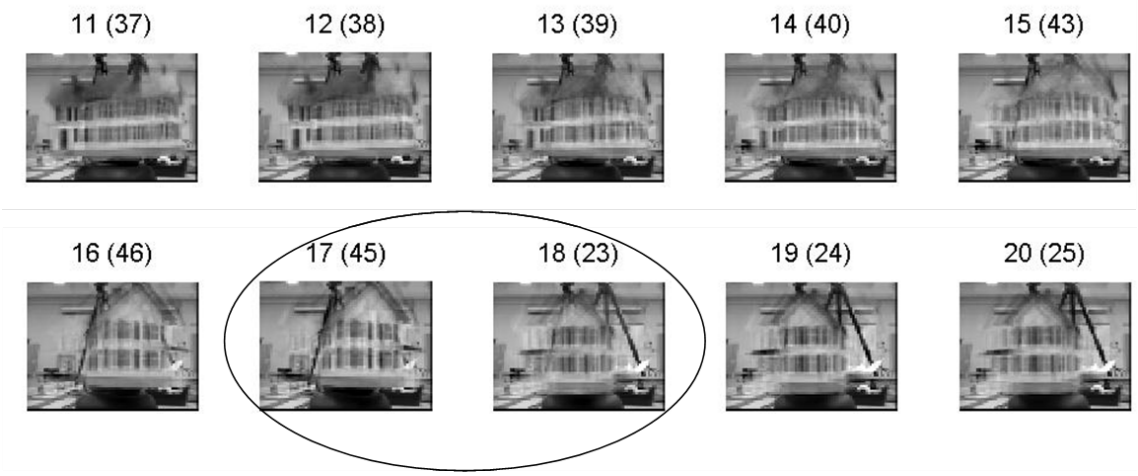

Figure 4.9: Image reconstruction using the first nine principal components for the house images. This image can be compared to that in Figure 4.6

The inability of PCA to choose the correct features can be seen in the reconstruction of the image sequences in Figures 4.7-4.8. These views look undistinguishable to a trained human eye. To verify the validity of ordering, the frame indices from the original video sequence are shown in parenthesis. These indices are referred to as, in Section 4.1, the "unscrambled" video sequence indices.

4.2.2 Two Cameras

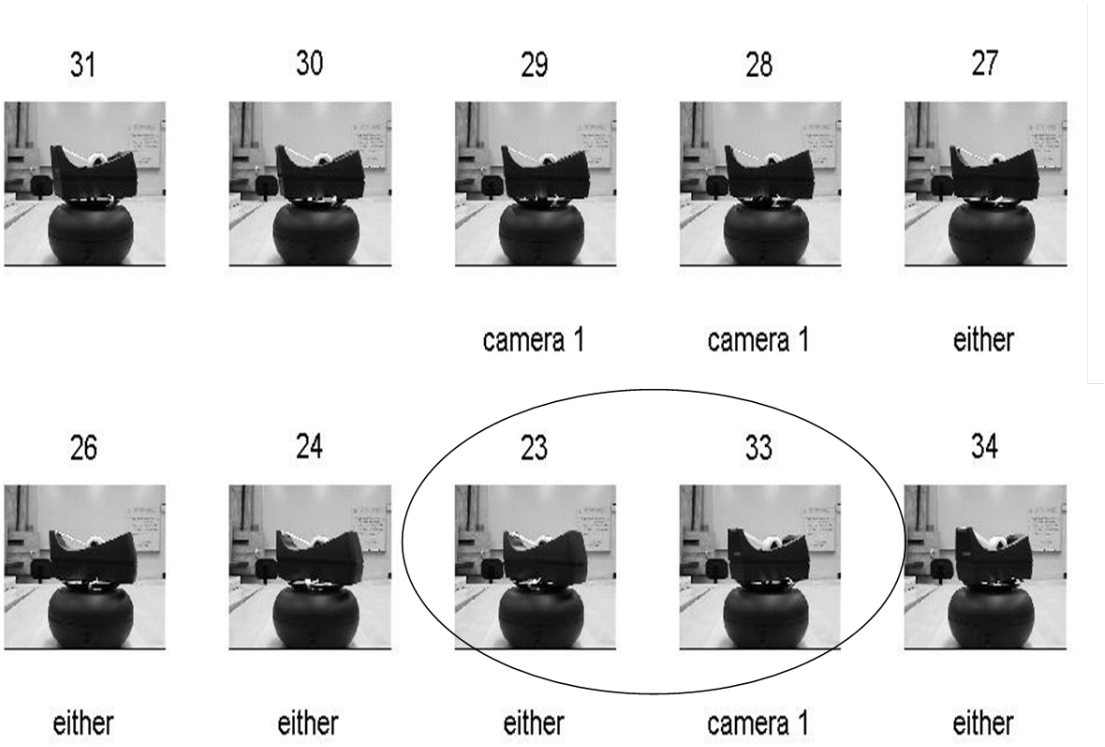

Figure 4.10: Example of a depth error induced from camera 1 confidence

This section will show image examples of how two camera ordering improves single camera ordering and the types of errors seen in using two cameras. Figure 4.10 show results of two camera ordering with a depth perception error. The error is a result from camera one similarity and camera two's inability to distinguish between front views. The view from camera two cannot be seen, but it is known that it is facing 90° apart from camera one which is facing the side. The two camera configuration is intended to switch to the camera with the most salient view for image ordering.

4.2.3 Eigenvalues v. Error Rate

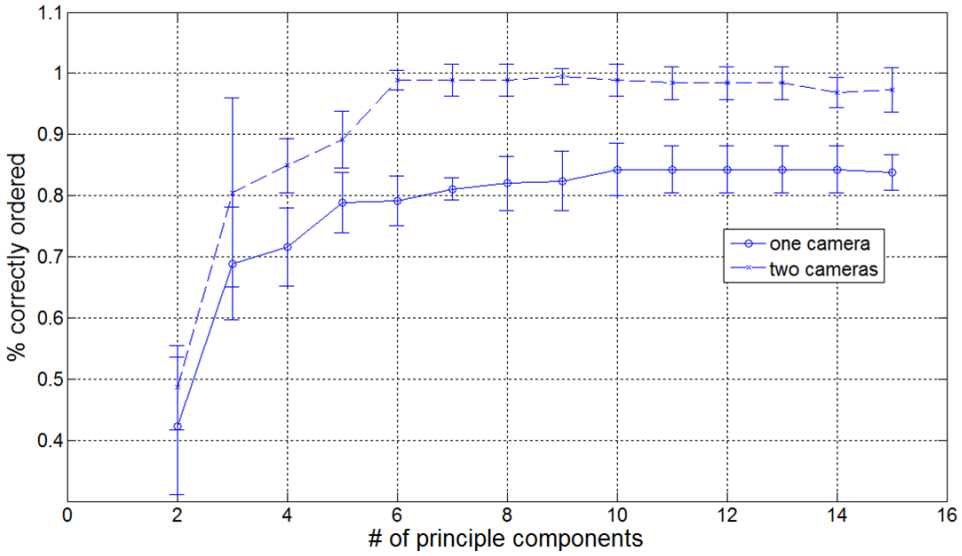

Figure 4.11: Number of principal components versus average error for an object. The standard deviation has been plotted for each trial.

Figure 4.11 represents the average error of pose ordering given a number of principal components. The average error has been taken over ten trials. Each trial has been given a different set of poses for the same object. From the plot in Figure 4.11 the optimum number of eigenvalues is nine. This is where the error rate reaches a limit and cannot be improved by adding more principal components. There is actually a slight decline in performance using higher dimensions. As mentioned in Section 3.1.2, 99% of the information explained by the variance is not enough to do accurate pose sequencing for all objects.

4.3 Laplacian Eigenmaps

In the previous section the object manifold was shown along with the analysis of errors in eigenspace. The Laplacian eigenmap method acts on the reduced space images of the manifold seen in the previous section. This method uses a Laplacian kernal to solve the eigenvalue problem seen in Section 2.3.2 on Laplacian eigenmaps. This section shows the results of the Laplacian eigenmap on the object manifold are clusters of image poses in the Laplacian eigenspace.

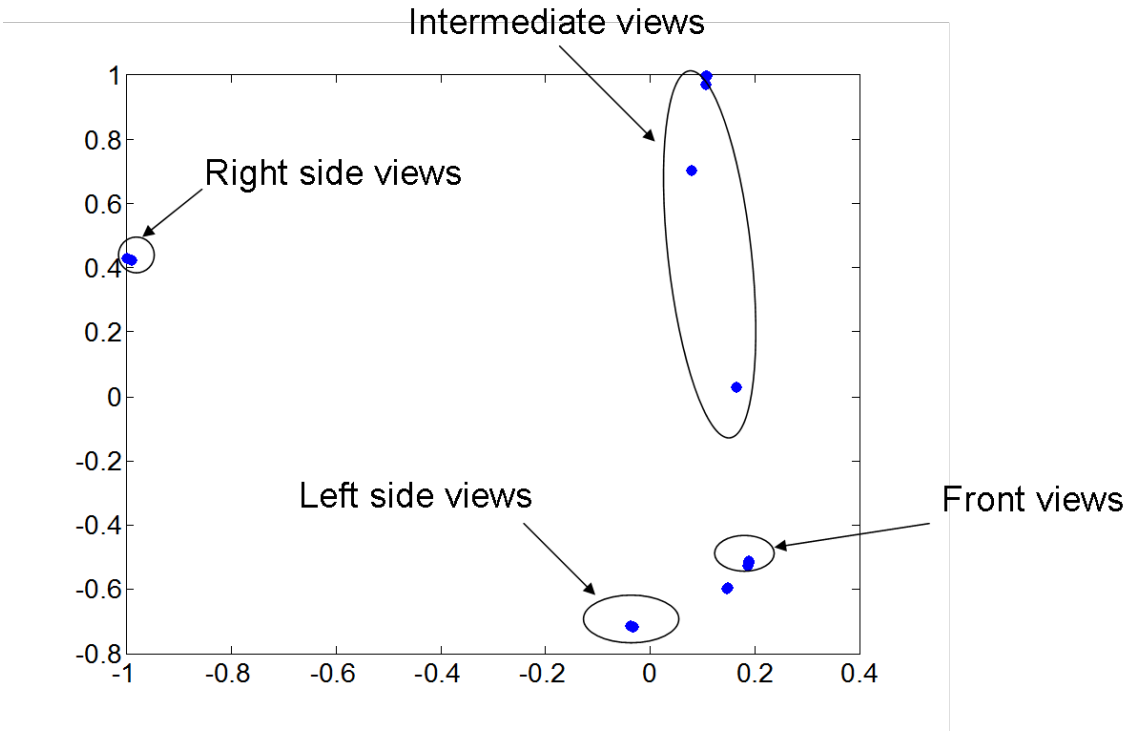

Figure 4.12: Laplacian eigenmap clustering t = 100

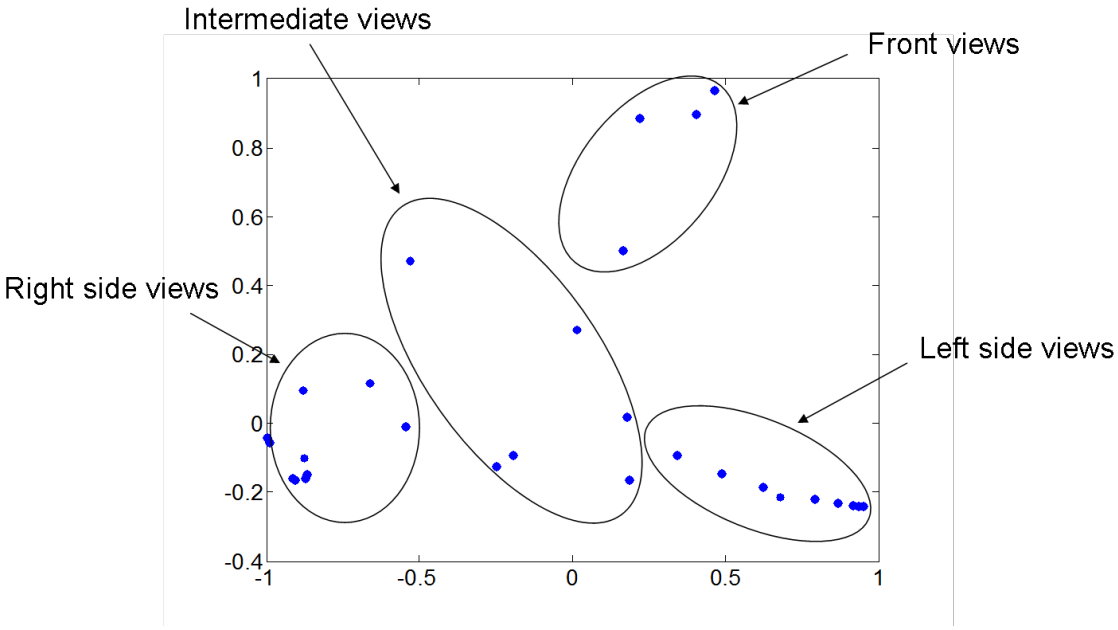

Figure 4.13: Laplacian eigenmap method t = 500

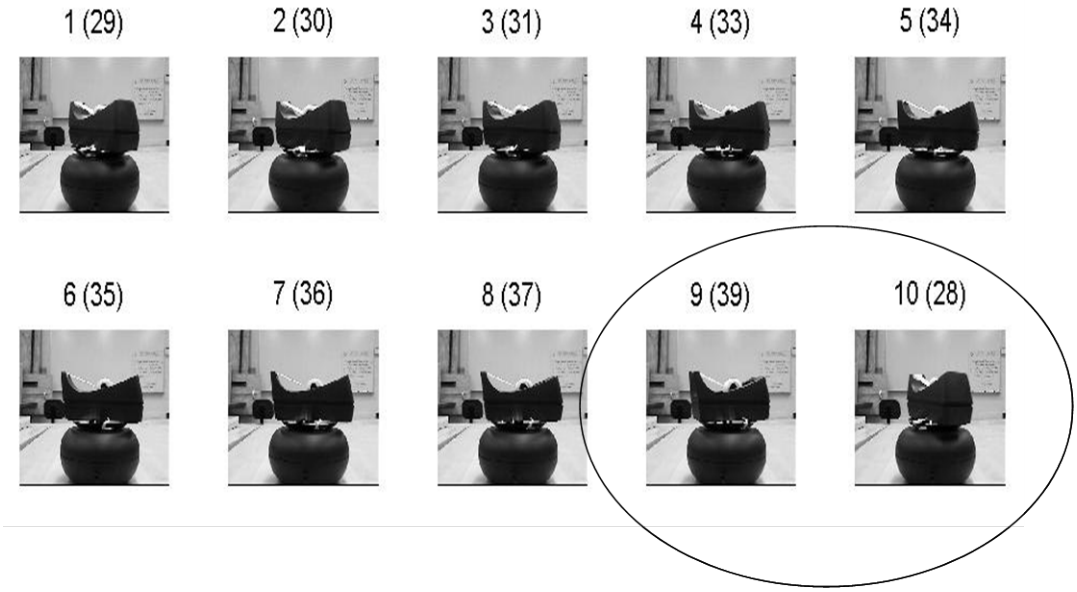

Figure 4.14: First 10 ordered images using Laplacian eigenmaps, t = 100

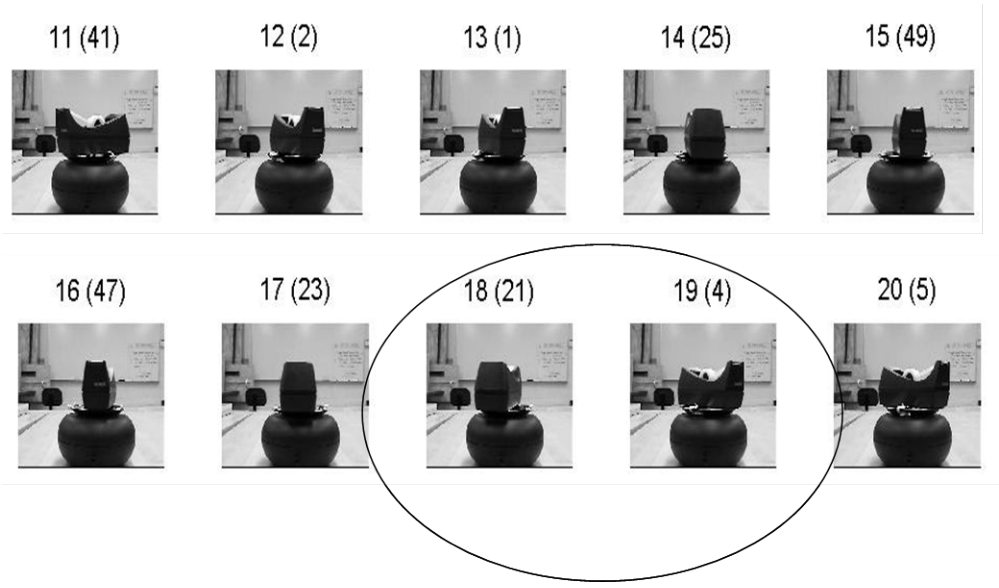

Figure 4.15: Ordered images 11 - 20 using Laplacian eigenmaps, t = 100

The first twenty ordered images, from the clusters seen in Figure 4.12, can be seen in in figures 4.14 and 4.15. The transition between pose clusters is indicated by the circled images. This is the region where a jump must be made from one pose cluster to another from the previously ordered image to the closest point in the next cluster. This is an undesired result because it is difficult to assess whether the pose is in the correct sequence. The Laplacian eigenmap method is primarily an unsupervised clustering algorithm to find a geometric solution to multidimensional data. Although this is a powerful method for unsupervised learning, it is not very useful for sequencing because the smooth manifold in eigenspace has been lost.

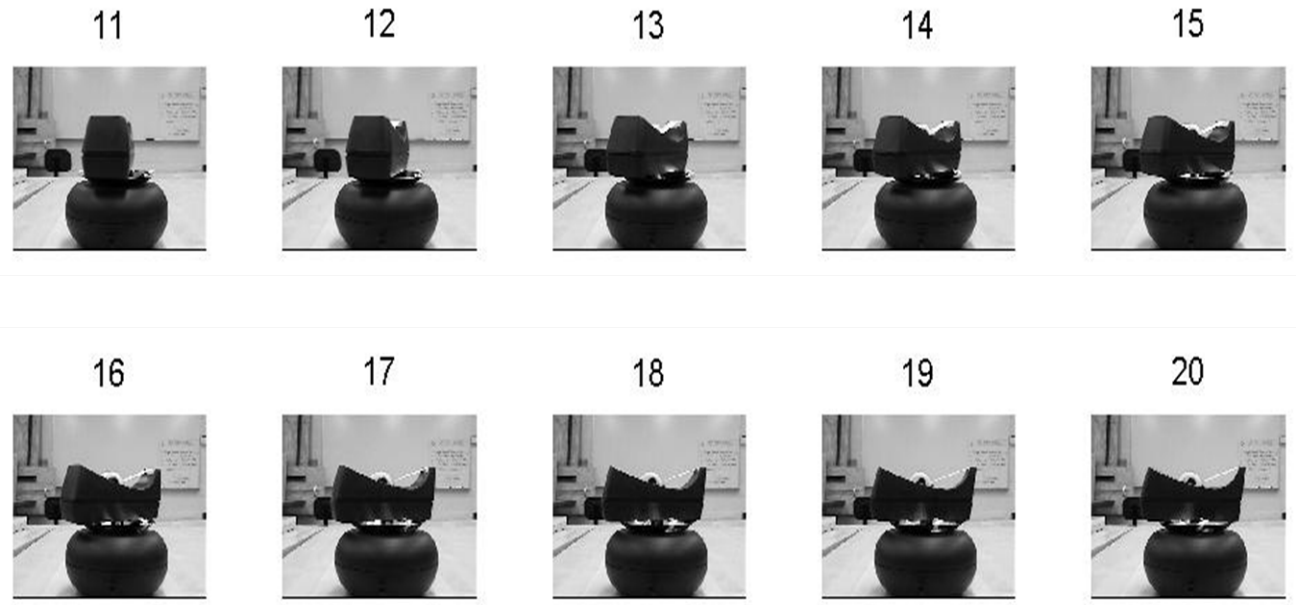

Figure 4.16: Single camera pose results for comparing the results of Laplacian eigenmaps

A comparison of the single camera method to the Laplacian eigenmaps helps to convey the idea of a smooth manifold. The types of errors from each method are distinctly different. Laplacian eigenmaps show errors of discontinuous views between the clusters and confusion of similar views resulting from dimensionality reduction. The PCA method contains errors just that of confusion of similar views due to dimensionality reduction. Figure 4.16 shows a smooth transition from front to intermediate view and intermediate to side views. The image sequence in 4.15 shows a jump from front views to side views that are apart approximately 90° in rotation. This sequence does not exhibit any transition to intermediate views before side views. The single camera PCA method clearly shows that it has no trouble with these types of transitions.

4.4 SIFT Results

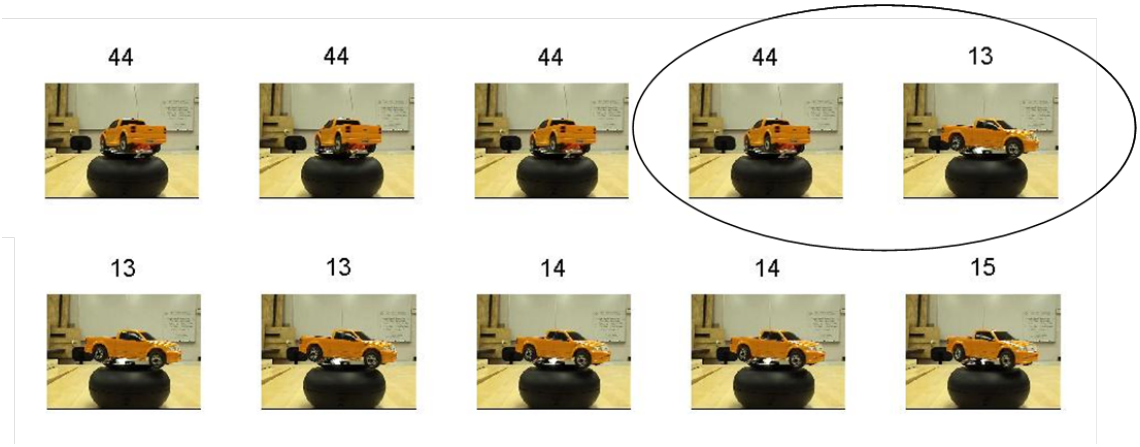

Figure 4.17: Results of the SIFT implementation for the tape dispenser images

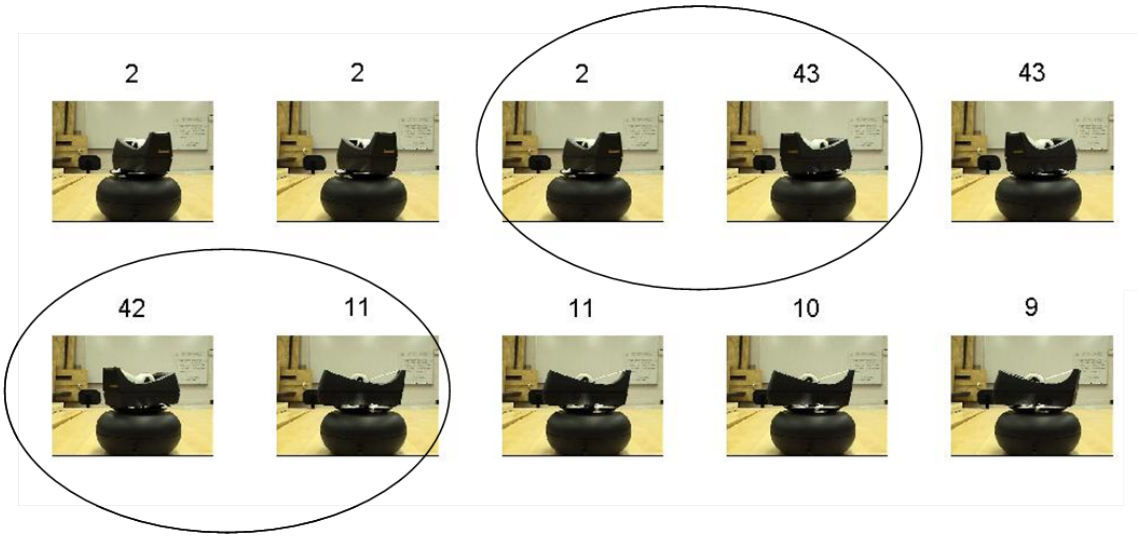

Figure 4.18: Results of the SIFT implementation for the truck images

The application of SIFT was found to not be useful for object pose ordering because similar matching keypoints were found between non-sequential pose views. Object sim-

ilarities around a 360° view confused the keypoint matching metric into finding many unlike views. This is a result of SIFT's inability to recognize objects in a scene exceeding a certain angled view. The illumination differences also cause too much confusion between similar keypoints. Results can be seen in Figures 4.4 and 4.4 with errors circled.

Chapter 5

Conclusion

5.1 Summary

This paper has outlined and specifically designed a method for ordering image poses of an object using a single or multiple camera architecture. PCA has been used as a basis for the algorithm because of its dimensionality reduction and feature extraction properties. Moreover, PCA has been used in multiple research applications for pose and object recognition (see Section 2). Data has been presented that shows the method from single camera ordering can be improved by adding an additional camera. A confidence metric has been developed that detects errors in ordering. The confidence metric is applied in eigenspace and allows for the fusion between two or multiple cameras. The fusion can be defined as choosing between cameras to find the best next view for ordering.

5.2 Future Work

Other applications for pose ordering such as path planning, which is used for controlling and monitoring moving objects, could be seen as a possible application. This is thought because the path of a vehicle or object that traverses a trajectory is a multidimensional manifold [23]. By using video frames, one could also embed a path into a reduced eigenspace. The manifold could be used to predict the controls of a vehicle [24]. The idea of using a camera based UAV control system has been presented in [25].

Bibliography

[1] A. Newman, "Face-recognition systems offer new tools, but mixed results," *New York Times*, 2001.

[2] D. G. Lowe, "Distinctive image features from scale-invariant keypoints," *International Journal of Computer Vision*, 2004.

[3] Y. Ke and R. Sukthankar, "Pca sift: A more distinctive representation for local image descriptors," *IEEE Conference on Computer Vision and Pattern Recognition*, 2004.

[4] J. Massaro and R. Rao, "Object pose ordering," *IEEE Conference on Acoustics, Speech, and Signal Processing*, 2009.

[5] S. O'Dwyer, P. Lewis, and J-P. Muller, "An application of stereomatching to the problem of geo-referencing historical air photos," *IEEE Conference on Remote Sensing*, 2003.

[6] M. Potuckova, "Image matching and it's application to photogrammetry," *Ph.D. Thesis Aalborg University*, 2004.

[7] L. Aryananda, "Online and unsupervised face recognition for humanoid robot: Toward relationship with people," *IEEE- RAS International Conference on Humanoid Robots*, 2001.

[8] W. Seales and O. Faugeras, "Building three dimensional object models from sequences," *Computer Vision and Image Understanding*, vol. 61, no. 3, pp. 308–324, 1995.

[9] A. Bottino and A. Laurentini, "Shape-from-silhouette when the relative position of the object is unknown," *TPAMI*, vol. 25, no. 11, pp. 1484–1493, 2003.

[10] K. Chueng, S. Baker, and T. Kanade, "Visual hull alignment and refinement across time: A 3d reconstruction algorithm combining shape-from-silhouette with stereo," *IEEE Conference on Computer Vision and Pattern Recognition*, 2003.

[11] T. Joshi, N. Ahuja, and J. Ponce, "Structure and motion estimation from dynamic silhouttes under perspective projection," *Int. Journal on Computer Vision*, pp. 290–295, 1995.

[12] M. Brown R. Szeliski and S. Winder, "Multi-image matching using multi-scale oriented patches," *IEEE Conference on Computer Vision and Pattern Recognition*, 2005.

[13] M. Brown and D. G. Lowe, "Unsupervised three dimensional object recognition and reconstruction in unordered data sets," *IEEE Conference on 3D Imaging and Modeling*, pp. 56–63, 2005.

[14] K. Grauman and T. Darrell, "Efficient image matching with distributions of local invariant features," *IEEE Conference on Computer Vision and Pattern Recognition*, vol. 2, no. 20, pp. 627–634, 2005.

[15] D. G. Lowe, "Object recognition from local scale-invariant features," *Proc. of the International Conference on Computer Vision*, pp. 1150–1157, 1999.

[16] D. Beymer, "Face recognition underying pose," *MIT Artificial Intelligence Laboratory*, , no. 89, 1993.

[17] H. Murase and S.K. Nayar, "Learning and recognition of 3d objects from appearance," *Int. J. of Comp. Vis.*, vol. 14, pp. 5–24, 1995.

[18] B. Moghaddam and A. Pentland, "Probabilistic visual learning for object representation," *TPAMI*, vol. 19, no. 7, pp. 696–709, 1997.

[19] J. Ham, I. Ahn, and D. Lee, "Learning a manifold-constrained map between image sets: applications to matching and pose estimation," *IEEE Conference on Computer Vision and Pattern Recognition*, 2006.

[20] Y. Rubner, C. Tomasi, and L. J. Guibas, "A metric for distributions with applications to image databases," *Proc. of the IEEE International Conference on Computer Vision*, 1998.

[21] R. Duda and P. Hart, *Pattern Classification*, Wiley-Interscience, New York, NY, 2nd edition, 2001.

[22] V. Perlibakas, "Distance measures for pca-based face recognition," *Pattern Recognition Letters*, vol. 25, pp. 711–724, 2004.

[23] C. Leung, S. Huang, and G. Dissanayake, "Active slam using model predictive control and attractor based exploration," *Inter. Conf. on Intelligent Robots and Systems IEEE/RSJ*, pp. 5026–5030, 2006.

[24] E. W. Frew, D. Lawrence, C. Dixon, J. Elston, and W. J. Pisano, "Lyapunov guidance vector fields for unmanned aircraft application," *Proc. of American Control Conference*, pp. 371–376, 2007.

[25] A. Kurdila, M. Nechyba, R. Prazenica, W. Dahmen, P. Binev, R. DeVore, and R. Sharpley, "Vision-based control of micro-air-vehicles: progress and problems in estimation," *43rd IEEE Conference on Decision and Control*, vol. 2, pp. 1635 – 1642, 2004.